Collisional processes involved in the population kinetics of semiconductor quantum-dot lasers

Janet L. Pan* and Peter L. Hagelstein
Research Laboratory of Electronics, Massachusetts Institute of Technology, Cambridge, Massachusetts 02139
(Received 2 July 1993)

We present an application to quantum dots of formulas from atomic physics for the rates of collisional ionization (binary encounter model) and dipole allowed collisional excitation (Van Regemorter and classical path models) occurring via the Coulomb interaction. The Van Regemorter, classical path, and binary encounter cross sections, which are known to be very successful in modeling atomic collisions, are shown to have accuracies comparable to (and are much easier to use than) the methods currently being used to study collisional rates in bulk excitons. Collisional excitation and ionization cross sections for a 150-Å-radius InSb quantum dot surrounded by CdTe barriers are shown to be much smaller than the geometric area πR^2, where R is the quantum-dot radius. The reason that these cross sections are so small is that the Coulomb energy associated with the collision is typically much smaller than the collisional energy exchange. Explicit formulas are given for quantum-dot intraband oscillator strengths.

I. INTRODUCTION

Recently, the quantization of the electron and phonon spectrum has been observed[1-5] in quantum dots of very small (tens of angstroms) radii. Quantum dots have previously been proposed for semiconductor lasers as a method of increasing laser efficiency[6,7] because the optical transitions between discrete bound energies could be spectrally very narrow. Further, the ability to make the typical separations between adjacent bound energy levels in a quantum dot large compared to $k_B T$ has led to speculation[7,8] that quantum-dot lasers could have characteristics (threshold gain and current density) which are much less temperature sensitive than conventional semiconductor lasers.

Since typical LO phonon energies in semiconductors have values on the order of the room temperature $k_B T$, the typical bound energy separations would exceed a LO phonon energy in the quantum dots just discussed. Thus, the bound carriers in these quantum dots are expected[9] to have little interaction with phonons. In a detailed model of the ionization balance which we will present in a future work, there are two ways in which we model phonon effects on the bound carriers in quantum dots having typical energy separations larger than a LO phonon energy. Acoustic phonons interact strongly with electrons whose energies are nearly degenerate and will force these electrons into a local thermal equilibrium. LO phonons in such quantum dots interact strongly only with those bound carriers which have energies within a LO phonon energy of the continuum. Bound state transitions resulting from LO phonon absorption or emission are very unlikely because bound energy separations will usually be very different from the nearly monochromatic LO phonon energy.

With the interaction of bound carriers with phonons inconsequential in such quantum dots, radiative (intraband as well as interband) and collisional (via the Coulomb interaction) processes involving bound carriers become important. Interband oscillator strengths[10,11] have already been discussed in the literature. Intraband dipoles are summarized in Appendix A. This paper studies the collisional excitation and ionization (and their inverse processes) of quantum-dot bound carriers caused by the Coulomb interaction between bound and free carriers (holes and electrons with energies in the continuum beyond the barrier band edge).

Quantum dots are more similar to atoms than they are to bulk or quantum well semiconductors in that the localized electrons in both atoms and quantum dots have discrete energies. Thus, some intuition about the processes important in quantum-dot population kinetics can be obtained from a study of ion plasmas. Of interest is the fact that in many astrophysical and laboratory plasmas,[12,13] the particle distribution among many of the excited levels in any particular atom or ion cannot be described by that of a Saha-Boltzmann equilibrium. In these cases, knowledge of the detailed collisional and radiative excitation and ionization rates are paramount in determining the population kinetics.

Our purpose for writing this paper is twofold. First, we make numerical estimates, based on well known ideas from ion plasmas, of collisional transition and ionization rates which we find to be important in the study of the population kinetics of semiconductor quantum-dot lasers when interaction with phonons can be ignored. In a future[14,15] paper, we will use these detailed collisional excitation (deexcitation) and ionization (recombination) processes affecting individual states to determine the validity of assuming[7-9,16-18] a quasiequilibrium, with its associated quasi-Fermi level, in each energy (conduction or valence) band in a quantum dot. We will find[14,15] that when interaction of bound carriers with phonons is negligible, the assumption of a quasiequilibrium in an energy (conduction or valence) band is not valid because all intraband (collisional and radiative) processes affecting bound states occur on a time scale much longer than an interband radiative lifetime.

The second purpose for writing this paper is to explore

the use in semiconductor problems of simple models from plasma physics for collisional transition and ionization affecting bound states. To this end, we compare the results from our simple models with experimental and other theoretical values of the collisional rates affecting semiconductor excitons. We find that the agreement with the literature is good.

We present in Sec. II A the first application to quantum dots of a Van Regemorter cross section for dipole allowed collisional excitation. Section II B and Appendix C present the classical path method, which is known to be useful for computing collisional excitation rates between strongly, intermediate, and weakly (dipole) coupled states in atomic plasmas. In Sec. III, we use a binary encounter theory to estimate quantum-dot collisional ionization rates. We checked that our collisional excitation and ionization cross sections agree with similar calculations from the literature for excitons and for atomic hydrogen in Secs. II C and III B. Explicit formulas are derived in Appendix A for intraband (as well as interband) oscillator strengths. Some of the integrals needed to compute collisional excitation and ionization rate coefficients are summarized in Appendixes B and D, respectively. We conclude with a summary of our work in Sec. IV.

To obtain numerical estimates throughout this paper, we will use the materials parameters for 150-Å-radii InSb quantum dots surrounded by CdTe barriers, which we have considered earlier[18] as a materials system whose Auger rate can be greatly reduced in comparison with the bulk. InSb has[19,20] a room temperature, bulk band gap of 163 meV, a spin-orbit splitting of 850 meV, a low frequency dielectric of $17.7\epsilon_0$, light hole, heavy hole, and conduction band effective masses at the Γ point of $0.015m_0$, $0.4m_0$, and $0.014m_0$, respectively. CdTe has a room-temperature[19,21–23] bulk conduction band edge which is 420 meV above that of InSb and a valence band edge which is 850 meV below that of InSb. CdTe has heavy hole and conduction band effective masses of $0.35m_0$ and $0.11m_0$, respectively, and a low frequency dielectric of $10.2\epsilon_0$. Unless otherwise specified, we will assume room-temperature operation of our quantum-dot lasers throughout this paper.

II. COLLISIONAL EXCITATION

Collisional excitation and deexcitation by incident electrons, can be indicated by the forward and reverse reactions, respectively ($E_{ji}>0$)

$$X(Z,i)+e \rightleftharpoons X(Z,j)+e \ . \tag{1}$$

A similar equation can be written for incident holes. Here $X(Z,i)$ denotes the quantum dot which has a total charge of Z on it and an electron (hole) in state i. (Unless explicitly stated otherwise, we will assume that we are dealing with neutral quantum dots in this paper.) In collisional excitation processes, the incident particle loses an energy E_{ji} as it excites a bound particle, via the Coulomb interaction between the two charged particles, in the quantum dot from state i to state j, as shown in Fig. 1. The collisional deexcitation rate coefficient q_{ji} is related to the collisional excitation rate coefficient q_{ij} through

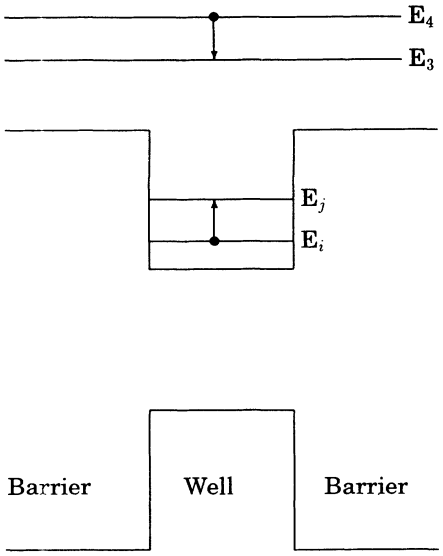

FIG. 1. In collisional excitation processes, the incident particle loses an energy $E_{ji}=E_{43}$ as it excites a bound particle, via the Coulomb interaction between the two charged particles, in the quantum dot from state i to state j.

the principle of detailed balance:

$$q_{ji}=\frac{g_i}{g_j}q_{ij}\exp\left[\frac{E_{ji}}{k_BT}\right], \tag{2}$$

where g_i is the degeneracy of the state i, and where we assume that the incident free particles have a Maxwellian distribution.

In this section, we will present collisional excitation cross sections obtained from two methods. The first uses a Van Regemorter[13,24] cross section and the second uses the classical path[13,25,26] (CP) (otherwise known as the impact parameter) method. Our purpose is to show that these two methods are much simpler to use than (and comparable in accuracy to) the ones currently being used to calculate collisional excitation cross sections for excitons (bound electron-hole pairs) in bulk semiconductors. Further, the simple analytical form of the Van Regemorter and classical path cross sections provides more immediate physical insight than numerically involved methods. The Van Regemorter and CP cross sections would also be very simple, numerically reliable methods of obtaining cross sections for collisional excitation in quantum dots.

Before presenting the Van Regemorter and classical path methods, we first summarize methods now being used to calculate collisional excitation cross sections in excitons. Cross sections for collisional excitation in bulk excitons by incident free carriers (electrons and holes) are often calculated using methods adapted from the study of scattering from the hydrogen atom, such as variational[27–29] techniques and the Glauber[30] approximation. Variational methods assume a particular form for the trial wave function, whose parameters are found by requiring the scattering phase shift[29] to be stationary. The

Glauber approximation appears to be the most successful[31] method of calculating collisional excitation in hydrogen and is thus quite useful for studying collisional excitation in bulk[30] excitons.

Results of the calculations based on the Glauber approximation for both hydrogen and excitons appear to be in good agreement with those based on variational methods. Honold *et al.*[32] and Schultheis *et al.*[33] found reasonable agreement (within a factor of 3) between these theoretical estimates of the collisional excitation cross sections for bulk excitons and those inferred from experiment.

These methods now being used to calculate cross sections for collisional excitation in bulk excitons are inconvenient to apply to the study of collisional excitation in quantum dots. For example, the Glauber approximation involves the computation of a cumbersome integral for each different transition $i \rightarrow j$. For the problem of scattering from bulk excitons, these cumbersome integrals are very similar to those calculated for scattering from the hydrogen atom. However, these Glauber integrals must be calculated anew for the quantum-dot scattering problem. Similarly, the variational results now being used for the excitonic scattering problem are almost identical to those for the hydrogenic scattering problem, but must be calculated anew for the quantum-dot scattering problem. The Van Regemorter and CP cross sections are much simpler to use since they involve only the computation of the oscillator strength, which is usually needed anyway.

The Van Regemorter (Sec. II A) and classical path (Sec. II B and Appendix C) cross sections are comparable in accuracy to the variational and Glauber methods in determining numerical values of the collisional excitation cross sections in realistic (Sec. II C) atomic or semiconductor systems. Figure 2 shows that both the Van Regemorter and CP cross sections are within a factor of 2 of the observed collisional excitation cross section in hydrogen. (This factor of 2 agreement is all that is needed for our purposes.[15]) We present in Fig. 3 the first application of these simple models to the collisional excitation of excitons in a bulk semiconductor. Our simple models agree with the more complicated Glauber approximation for the collisional excitation in bulk excitons. This success of the Van Regemorter and CP methods allows us to predict quantum-dot collisional excitation cross sections, of which experimental measurements are not available at present, as in Figs. 4 and 5.

The use of the Van Regemorter and CP cross sections also provides insight not immediately available from the variational or Glauber techniques. For example, we find the curious result, which will be explained later in this section, that the quantum-dot collisional excitation cross section is much smaller than the physical size πR^2. From the Glauber and variational results mentioned above, one would not understand this, since the collisional excitation cross sections in bulk excitons are always on the order of the physical size $\pi a_{\rm ex}^2$, where $a_{\rm ex}$ is the exciton Bohr radius. As we will discuss in more detail below, the collisional excitation cross sections in quantum dots are much smaller than the physical size πR^2 because the typical Coulomb energy involved in the collision is much smaller than the typical collisional excitation energy, an observation which will be clear from the Van Regemorter and CP formulas.

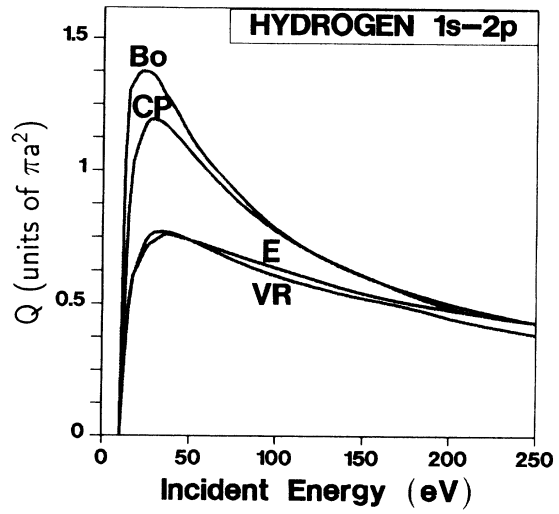

FIG. 2. The collisional excitation cross section, in units of πa_0^2, where a_0 is the Bohr radius, as a function of incident electron energy for the 1*s*-2*p* transition in hydrogen. The experimental (E) data and the calculation in the Born (Bo) approximation are taken from Seaton's (Ref. 25) paper. The results of the classical path (CP) method (using a cutoff radius of $2.008a_0$) are obtained from Eq. (64). The Van Regemorter (Ref. 24) cross section is obtained using Eq. (7).

We emphasize that the power of our Van Regemorter and classical path models lie both in their simplicity and

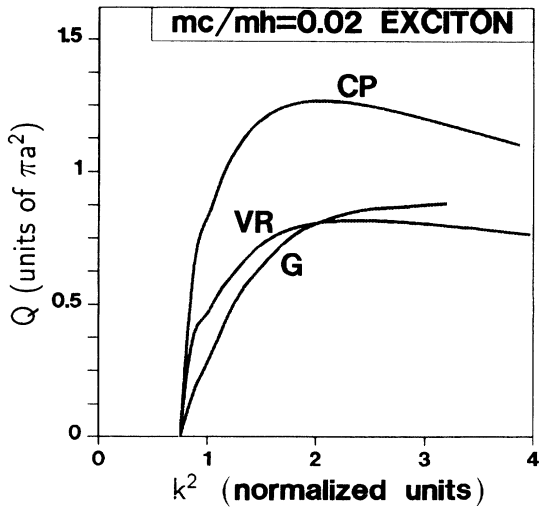

FIG. 3. The collisional excitation cross section as a function of incident electron energy for the 1*s*-2*p* transition in an exciton in a semiconductor, such as CdS, with $m_c/m_h=0.02$. The results of the Glauber approximation (G), known to be very successful in predicting collisional excitation rates in hydrogen, were calculated (Ref. 30) by Elkomoss and Munschy for excitons in many semiconductors. For comparison, we calculate this same cross section using the (CP) method (using a cutoff radius of $2.008a_{\rm ex}$, where $a_{\rm ex}=(1+m_c/m_h)a$[EM]) of Eq. (C8) and the Van Regemorter (VR) cross section of Eqs. (7) and (22).

in their ability to provide numerics of comparable accuracy to what is now being used in studying bulk excitons.

A. Van Regemorter collisional excitation rates

The matrix element for the Coulomb interaction between the incident and bound particles is

$$V_{ji}=\left\langle I\left|\frac{e^2}{4\pi\epsilon_{ce}|\mathbf{r}'-\mathbf{r}|}\right|F\right\rangle=\left\langle j,1\left|\frac{e^2}{4\pi\epsilon_{ce}|\mathbf{r}'-\mathbf{r}|}\right|i,1'\right\rangle , \tag{3}$$

where $\mathbf{r},\mathbf{r}'$ are the coordinates of the bound and incident particles, respectively, where I, F are the total (free particle plus quantum dot) initial and final states, where j,i are the initial and final bound particle states, and where $1,1'$ are the initial and final free particle states.

1. Van Regemorter cross sections

When the incident particle does not penetrate the quantum dot, the largest contribution to the collisional excitation rate is for dipole allowed bound state transitions. In such cases, (3) can be approximated as the product of the dipole between the bound states i,j and the electric field of the incident particle as seen by the bound particle. When the incident particle penetrates the target, the classical path model, discussed later in this paper, can be used.

The Van Regemorter[24] collisional excitation cross section for dipole allowed transitions, modified to include the materials parameters of our semiconductor quantum-dot system, is

$$Q(i\rightarrow j)=\left[\frac{2\pi}{\sqrt{3}}\right]\left[\frac{m_i}{m_0}\right]\left[\frac{\sum_{\text{degenerate } i,\ \text{degenerate } j} f_{ji}}{3g_i}\right]\left[\frac{g_G}{E_{ji}E_{\text{inc}}}\right]\left[\frac{e^2}{4\pi\epsilon_{ce}R}\right]^2(\pi R^2) , \tag{4}$$

where the effective mass m_i is that of the incident particle, R is the radius of the quantum dot, and E_{inc} is the incident particle energy (measured from the band edge of the barrier material). The oscillator strength f_{ji} and the Gaunt factor g_G are discussed later in this section.

Some discussion is necessary as to the appropriate dielectric constant to use in (4) for a distant encounter between the incident particle in the barrier region, whose low frequency dielectric is ϵ_{bar}, and the bound particle in the quantum dot, whose low frequency dielectric is ϵ_{QD}. We propose to use in (4) the dielectric constant ϵ_{ce} which we define to be

$$\epsilon_{ce}=\tfrac{1}{3}(\epsilon_{\text{QD}}+3\epsilon_{\text{bar}}) \tag{5}$$

for collisional excitation cross sections. Equation (5) is obtained by observing that the electric field of the incident particle in a distant encounter with the quantum dot corresponds to a roughly uniform electric field inside the quantum dot which is $3\epsilon_{\text{bar}}/(\epsilon_{\text{QD}}+2\epsilon_{\text{bar}})$ times[34,35] that of the roughly uniform electric field, proportional to $e^2/4\pi\epsilon_{\text{bar}}$, just outside the quantum dot in the barrier region.

(a) Gaunt factors. The Gaunt factor is defined as

$$g_G=\frac{8}{\sqrt{3}}\sum_{\mu}|\langle 1|r^{-2}Y_{1\mu}|1'\rangle|^2 \tag{6}$$

and is associated with the electric field of the incident particle. We take the Gaunt factor g_G in (4) to be that given for neutral targets in Table 1 of Van Regemorter's paper.[24] Van Regemorter's Gaunt factor was chosen to match the measured $1s$-$2p$ collisional excitation cross section in hydrogen. To within 5%, we can accurately approximate this Gaunt factor as

$$g_G=\begin{cases}0.073\left[\frac{E_{\text{inc}}}{E_{ji}}-1\right]^{1/2}+0.051\left[\frac{E_{\text{inc}}}{E_{ji}}-1\right]^{3/2} & \text{for } E_{ji}<E_{\text{inc}}<2E_{ji}\\ \dfrac{\left\{\left[\frac{\sqrt{3}}{2\pi}\ln|x_0^2+1|-0.124\right]\left[\frac{E_{\text{inc}}}{E_{ji}}-1\right]^{1/2}+\left[0.124x_0-\frac{\sqrt{3}}{2\pi}\ln|x_0^2+1|\right]\right\}}{x_0-1} & \text{for } 2E_{ji}<E_{\text{inc}}<(x_0^2+1)E_{ji}\\ \frac{\sqrt{3}}{2\pi}\ln\left|\frac{E_{\text{inc}}}{E_{ji}}\right| & \text{for } E_{\text{inc}}>(x_0^2+1)E_{ji} ,\end{cases} \tag{7}$$

where we choose $x_0=4$ to match the large incident energy limit of the correct Gaunt factor as given by Van Regemorter and by Burgess and Tully.[36]

(b) Oscillator strengths. In intraband transitions, the dipole operator acts on the envelope part of the particle wave functions. A more complete discussion and derivation of the intraband dipoles and oscillator strengths $f_{ji}\equiv(2m_0E_{ji}/\hbar^2)|\langle i|\mathbf{r}|j\rangle|^2$ to be used in (4) is given in Appendix A.

(c) Relation to bulk processes. Depending on whether the incident particles are electrons (with its associated rate $n_c q_{ij}^c$) or holes (with its associated rate $n_v q_{ij}^v$), these collisional excitation processes, as well as the collisional ionization processes discussed below, are analogous to what is termed[37] electron-electron, hole-hole, or electron-hole Coulomb scattering in the bulk. Observe that in electron-hole scattering, the two initial (and whence, the two final particles) are not in the same energy (conduction or valence) band. Electron-hole scattering is known to be important in the bulk for small band-gap semiconductors such as InSb.

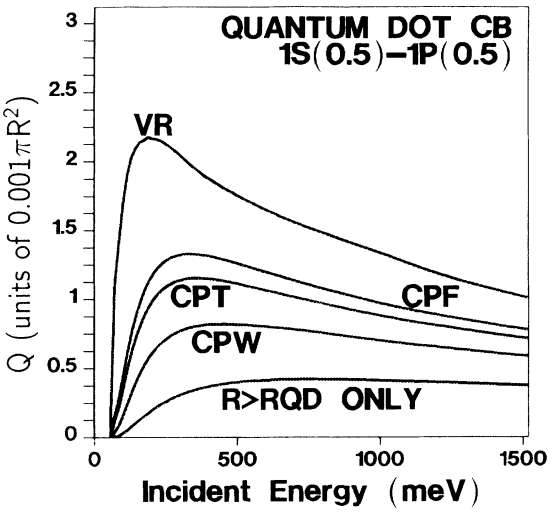

FIG. 4. The collisional excitation cross section (units of $0.001\pi R^2$) as a function of incident electron energy at room temperature for the $1S_{1/2}$-$1P_{1/2}$ transition in the conduction band of a 150-Å-radius InSb quantum dot surrounded by CdTe barriers. The weak (CPW) and intermediate (CPF,CPT) forms of the CP method, obtained from (62), (70), and (71) [with (63) calculated to be $0.6R$], were obtained using the correct dielectric everywhere: $\epsilon=\epsilon_{\rm QD}$ when the incident particle is inside the quantum dot and $\epsilon=\epsilon_{ce}$ otherwise. The contribution from impact parameters greater than R, labeled $R>RQD$, is seen to be much smaller than the CP cross sections, thus indicating that the largest contributions to collisional excitation are from near collisions. The neglect of the difference in dielectric between the quantum dot and barrier materials makes the Van Regemorter (VR) cross section, obtained from (4) and (7), much larger than the CP cross sections. The difference in the heights of the CPW, CPT, and CPF curves is a rough estimate of the errors incurred in estimating the contributions of the very near collisions using the CP method. The small size of the quantum-dot collisional excitation cross section relative to the physical size πR^2 is a result of the fact that E_{ji} is much larger than the typical Coulomb energy ($e^2/4\pi\epsilon_{ce}R$). (See text.)

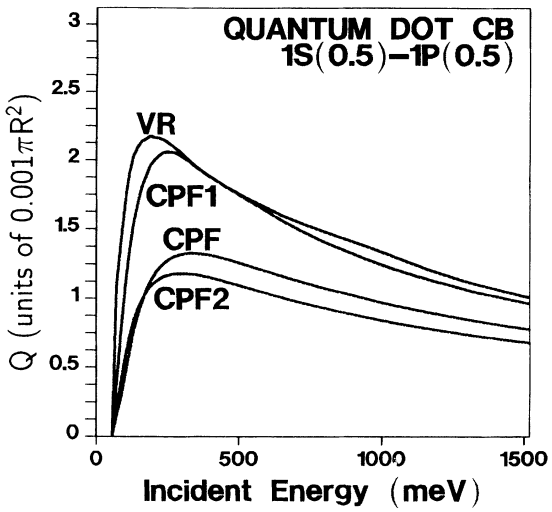

FIG. 5. The effect of the difference in the quantum dot and barrier dielectric constants on the collisional excitation cross section. CPF is the correct curve calculated from the CP method [with (63) calculated to be $0.6R$] with $\epsilon=\epsilon_{ce}$ when the incident particle is outside the quantum dot and $\epsilon=\epsilon_{\rm QD}$ when the incident particle is inside the quantum dot. The curve labeled CPF2 is calculated from the CP method (75) with $\epsilon=\epsilon_{ce}$ for those incident particle paths with impact parameter greater than R, and $\epsilon=\epsilon_{\rm QD}$ *everywhere along* those incident particle paths with impact parameter less than R. CPF and CPF2 are similar because the dominant contribution to the cross section when the impact parameter is less than R occurs when the incident particle is inside the quantum dot. The curve labled CPF1 is calculated from the CP method with $\epsilon=\epsilon_{ce}$ for all incident particle paths. Thus, it is very similar to the Van Regemorter cross section of Fig. 4, which also uses $\epsilon=\epsilon_{ce}$ everywhere along the incident particle trajectory.

In Appendix A, we observed that collisional processes involving an interband transition are much weaker than those involving only intraband transitions. Though we will *not* be considering such collisional excitation processes which involve an interband transition, we observe that the analogous process in the bulk is called[37] an impact ionization or inverse Auger process: the energy (which is at least the band gap energy) lost by the incident electron (or incident hole) promotes an electron (hole) from the valence (conduction) to the conduction (valence) band.

2. *Van Regemorter rate coefficients*

The collisional excitation rate is

$$n_{c,v}q_{ij}^{c,v}\equiv n_{c,v}\langle Q(i\rightarrow j)v\rangle = \int Q(i\rightarrow j)v g_{c,v}(E)f_{c,v}(E)dE\ , \tag{8}$$

where $v=(2E/m_{C,V}^{\rm bar})^{1/2}$, where the Fermi-Dirac occupation probabilities of the free electrons and the free holes, whose respective concentrations are $n_{c,v}$, can be approximated as Maxwellian in the nondegenerate limit,[38]

$$f_{c,v}(E)=\frac{1}{1+\exp\left[\dfrac{E-E_{Fc,Fv}}{k_BT}\right]}\simeq\frac{n_{c,v}}{N_{C,V}}\exp\left[\frac{-E}{k_BT}\right], \tag{9}$$

where $N_{C,V}=2(2\pi k_BT/h^2)^{3/2}m_{\mathrm{DOS},C,V}^{\mathrm{bar}(3/2)}$, where

$$m_{\mathrm{DOS},C}^{\mathrm{bar}(3/2)}=m_c^{3/2},$$
$$m_{\mathrm{DOS},V}^{\mathrm{bar}(3/2)}=(m_{\mathrm{LH}}^{3/2}+m_{\mathrm{HH}}^{3/2}), \tag{10}$$

where E is measured from the band edge of the barrier material and the density of final stages $g(E)$ for the free particles is the bulk density of states (DOS) (per unit volume) in the *barrier* material having a specific spin

$$g_{c,v}(E)=\frac{1}{4\pi^2}\left[\frac{2m_{\mathrm{DOS},C,V}^{\mathrm{bar}}}{\hbar^2}\right]^{3/2}E^{1/2}. \tag{11}$$

Using (4) and (8), we can write the collisional excitation rate as

$$n_{c,v}q_{ij}^{c,v}=n_{c,v}(R^2v_{th})\left[\frac{e^2}{4\pi\epsilon_{ce}R}\right]^2\left[\frac{(3\pi^3)^{-1/2}}{E_{ji}k_BT}\right]\left[\frac{m_i}{m_0}\right]\left[\frac{\sum_{i,j}f_{ji}}{3g_i}\right]P_{\mathrm{VR}}\left[\frac{E_{ji}}{k_BT}\right], \tag{12}$$

where

$$v_{th}=\left[\frac{2k_BT}{m_i}\right]^{1/2} \tag{13}$$

and where we used Van Regemorter's notation to define the integral

$$P_{\mathrm{VR}}\left[\frac{E_{ji}}{k_BT}\right]=\int_{E_{ji}/k_BT}^{\infty}d\mathcal{E}\exp(-\mathcal{E})g_G(\mathcal{E}), \tag{14}$$

where $\mathcal{E}=E_{\mathrm{inc}}/k_BT$ and g_G is the Van Regemorter Gaunt factor (7). The integral in (14) is carried out in Appendix B, wherein appropriate limiting forms of the integral are also given.

B. The classical path method

Before presenting numerical values for the cross sections for collisional excitation in a hydrogen atom, an exciton in a bulk semiconductor, and a quantum dot, we briefly discuss the collisional excitation cross sections obtained from the classical path method. As discussed more fully in Appendix C, the classical path method is extremely useful in situations where the collisional excitation cross section is dominated by the near collisions, which involve small impact parameters. This could occur when the bound states involved are strongly dipole coupled, for which the Born and Van Regemorter collisional excitation cross sections are often much larger than observed cross sections. In such cases, Seaton[25] has shown that much better agreement with experiment is obtained from a strong coupling limit of the classical path method, in which the transition probabilities for small impact parameters are limited to physically accessible values (less than unity). The collisions which penetrate the electronic orbits surrounding an ion make important contributions to the collisional excitation cross section in highly stripped ions, for which Hagelstein[39] has found very good agreement with experiment from an intermediate coupling form of the classical path model.

One of the advantages of the classical path method lies in its simplicity, especially in its treatment of collisional excitations dominated by contributions from small impact parameters. The other advantage of the classical path method is that, as is shown[15] in the literature, it is numerically accurate (to within a factor of 2) enough for our purpose of determining the conditions under which quasiequilibrium exists within a quantum-dot energy band. A more complete discussion of the classical path method is given in Appendix C. We present a summary here.

In the limit in which the bound states i,j are weakly coupled, the classical path collisional excitation cross section is dominated by collisions having large impact parameters and is given by (C8)

$$Q_{\mathrm{CPW}}(i\rightarrow j)=\left[\frac{m_i}{m_0}\right]\left[\frac{2\sum_{i,j}f_{ji}}{3g_i}\right]\left[\frac{1}{E_{ji}E_{\mathrm{inc}}}\right]\times\left[\frac{e^2}{4\pi\epsilon_{ce}R}\right]^2\phi(\beta_{\mathrm{co}})(\pi R^2), \tag{15}$$

where β_{co} is (C4) evaluated at the cutoff impact parameter R_{co}, and where the function $\phi(\beta_{\mathrm{co}})$ is given in Eq. (C9). The cutoff impact parameter R_{co} is chosen to be the physical size of the target, which we define as the root mean square orbit size of the i,j states (C7). This choice of cutoff impact parameter is physically reasonable for many target[39] atoms and it allows the CP cross sections to match the experimentally observed high energy limit of the collisional excitation cross section.

In the limit in which the bound states i,j are strongly coupled, the classical path collisional excitation cross section is given by (C13)

$$Q_{\mathrm{CPS}}(i\rightarrow j)=\left[\frac{m_i}{m_0}\right]\left[\frac{2\sum_{i,j}f_{ji}}{3g_i}\right]\left[\frac{1}{E_{ji}E_{\mathrm{inc}}}\right]\times\left[\frac{e^2}{4\pi\epsilon_{ce}R}\right]^2[\phi(\beta_1)+\tfrac{1}{2}\zeta(\beta_1)](\pi R^2)\ , \tag{16}$$

where $\zeta(\beta_1)$ is given in Eq. (C5), β_1 is (C4) evaluated at R_1, and R_1 is the cutoff impact parameter, defined in (C11), which limits the transition probability to physically accessible values for those collisions having small impact parameters.

The intermediate[39] form of the CP model will be used in this paper to describe collisional excitations dominated by near collisions, as in highly stripped ions[39] and, as we shall see, in quantum dots. The intermediate[39] form of the CP cross section is obtained from the assumption that the transition probabilities at small impact parameters are similar to those at the cutoff impact parameter, as in (C14). The collisional excitation cross section is thus

$$Q_{CPT}(i\rightarrow j)=\left[\frac{m_i}{m_0}\right]\left[\frac{2\sum_{i,j}f_{ji}}{3g_i}\right]\left[\frac{1}{E_{ji}E_{\mathrm{inc}}}\right]\times\left[\frac{e^2}{4\pi\epsilon_{ce}R}\right]^2[\phi(\beta_{\mathrm{co}})+\tfrac{1}{3}\zeta(\beta_{\mathrm{co}})](\pi R^2)\ . \tag{17}$$

Another intermediate[39] form of the CP cross section is given in Appendix C. Appendix C also shows how the difference in the quantum dot and barrier dielectrics can be approximately accounted for.

C. Numerical evaluation

In this subsection, we use our formulas above to calculate CP and Van Regemorter cross sections and rate coefficients for collisional excitation by electron impact in a hydrogen atom, in an exciton in a bulk semiconductor, and in a quantum dot. Our purpose for presenting these numerical values is to demonstrate that Van Regemorter and classical path formulas are very simple models which nevertheless provide reliable numerics. We recapitulate the success that these simple models have had in astrophysics by studying collisional excitation in hydrogen. Next, we present the application of these simple models to the collisional excitation in bulk excitons, for which we demonstrate good agreement with other theoretical and experimental results. Finally, we apply our model to collisional excitation in quantum dots, for which our purpose is to estimate rate coefficients.

1. Calculations for hydrogen

Figure 2 shows the collisional excitation cross section, in units of πa_0^2 where a_0 is the Bohr radius, as a function of incident electron energy for the $1s$-$2p$ transition in hydrogen. The experimental (E) data and the calculation in the Born (Bo) approximation are taken from Seaton's[25] paper. The results of the CP method are obtained from Eq. (C8). The Van Regemorter (VR) cross section in Fig. 2 is obtained using Eqs. (4) and (7). For the $1s\rightarrow 2p$ transition in hydrogen, the oscillator strength and excitation energy are[25]

$$f_H=\left[\frac{\sum_{i,j}f_{ji}}{3g_i}\right]=0.416,\quad E_{H,ji}=\tfrac{3}{4}I_H\ , \tag{18}$$

where I_H is the ionization potential of hydrogen.

The cutoff radius for the classical path calculation, which is the root mean square radius in the $1s$ and $2p$ states (about 2.008 Bohr radii), allows the CP cross section to match measured cross sections in the limit of large incident energies. This is what we would expect since the integration in (C6) should not include the near collisions, for which the weak coupling limit of the CP model is not appropriate. The $1s$-$2p$ oscillator strength is rather large: the transition probability (C3) at incident energies near threshold is about 0.2. If the CP weak coupling limit were no longer applicable, the strong or intermediate forms of the CP method would be invoked to ensure that transition probabilities remain physically reasonable.

That the van Regemorter cross section of Eqs. (4) and (7) is very similar to the experimental data is not surprising since Van Regemorter's Gaunt factor was chosen to match this particular transition in H. That Fig. 2 shows the classical path cross section to be very similar to the Born approximation is also not surprising since both are based on similar assumptions and both are expected to be more accurate for large incident energies. What is a bit surprising is that, even at energies near threshold, our classical path cross section is well within a factor of 2 of the measured cross section. This is a powerful result, given the great simplicity of the CP model.

One might argue that errors of the order of 50% may render the Van Regemorter cross sections useless. However, for the best part of 30 years, a 50% accuracy was acceptable[25] in the atomic plasma community. Further, for our purpose of determining[15] the quantum-dot population kinetics, this 50% error is inconsequential to our main result; we find[15] that only errors worse than *five* orders of magnitude would change our qualitative result.

2. Calculations for excitons

We now compare our Van Regemorter and CP cross section with the $1s\rightarrow 2p$ collisional excitation cross section in excitons for incident electrons as calculated by Elkomoss and Munschy[30] in the Glauber approximation. The Glauber approximation has had much success[31] in predicting cross sections for scattering off hydrogenic ions at intermediate and large incident energies. This should serve to calibrate the accuracy of our simple model for a semiconductor system.

Our Van Regemorter cross section is, using (4),

$$Q(i\rightarrow j)=\left[\frac{8\pi}{\sqrt{3}}\right]\left[\frac{m_i}{m_0}\right]\left[\frac{\sum_{i,j} f_{ji}}{3g_i}\right]\left[\frac{I_{\rm ex}}{E_{ji}}\right]\times\left[\frac{I_{\rm ex}}{E_{\rm inc}}\right]g_G(\pi a_{\rm ex}^2)\ , \tag{19}$$

where $I_{\rm ex}=m_r e^4/2\hbar^2(4\pi\epsilon)^2$ is the ionization energy of an exciton and $a_{\rm ex}=\hbar^2(4\pi\epsilon)/m_r e^2$ is the exciton radius. In keeping with the notation of Elkomoss and Munschy, we define the effective mass ratio

$$\sigma=\frac{m_c}{m_h}\ , \tag{20}$$

which allows the reduced mass to be written as

$$m_r=\frac{m_c}{1+\sigma}\ . \tag{21}$$

Accounting for the effective masses and dielectric in a semiconductor, we can write $I_{\rm ex}=(m_r/m_0)(I_H/\epsilon^2)$, $E_{ji,\rm ex}=\frac{3}{4}I_{\rm ex}$, $(m_r/m_0)f_{ji,\rm ex}=f_H$, $m_i=m_c$. Using the notation of Elkomoss and Munschy for the normalized incident energy, we write $E_{\rm inc}=(1+2\sigma)k_i^2 I_{\rm ex}$. The Van Regemorter cross section, obtained using (7), is then

$$Q(i\rightarrow j)=\left[\frac{8\pi}{\sqrt{3}}\right]\left[\frac{\frac{4}{3}}{(1+2\sigma)k_i^2}\right]\times(0.416)(1+\sigma)^3 g_G(\pi a_{0,\rm EM}^2)\ , \tag{22}$$

where the exciton radius is related to the length $a_{0,\rm EM}$ defined by Elkomoss and Munschy through $a_{\rm ex}=(1+\sigma)a_{0,\rm EM}$.

A numerical comparison of our Van Regemorter (22) and CP cross sections with the cross sections of Elkomoss and Munschy[30] (labeled G for Glauber) is given in Fig. 3. The parameter given, $\sigma=0.02$, corresponds[30] to CdS. The largest value of k_i^2 presented in our figure is the largest one for which Elkomoss and Munschy gave a collisional excitation cross section. For values of incident energy much larger than the ones given, we expect very good agreement, as the cross sections predicted by all reasonable theories approach the Bethe approximation as given by Burgess and Tully.[36]

At incident energies shown in Fig. 3, the agreement between our Van Regemorter cross section and the Glauber cross section of Elkomoss and Munschy is extremely good. This should not be surprising in view of Fig. 2, since the equations describing the 1s-2p collisional excitation in this bulk exciton are almost identical to those for the hydrogen atom.

The cutoff radius used in the CP calculation of Fig. 3 was taken to be 2.008 exciton Bohr radii, by analogy with the hydrogen collision problem above, since $m_c \ll m_h$. For the CP calculations, the agreement between our results and theirs is about 40% at intermediate incident energies. Again, this is similar to the agreement between the CP method and experiment which we saw in Fig. 2 for atomic hydrogen. The largest discrepancies between the CP and the Glauber calculations appear at incident energies near threshold. This is to be expected, as it is well known[31] that the Glauber approximation underestimates and that the Born approximation overestimates the collisional excitation cross sections near threshold.

Given the extreme simplicity of our CP and Van Regemorter models, this agreement with the Glauber calculation of the collisional excitation in bulk excitons is quite satisfactory. Honold *et al.*[32] and Schultheis *et al.*[33] found reasonable agreement between the Glauber approximation in bulk excitons and collisional excitation cross sections inferred from experiment.

3. *Calculations for quantum dots*

The discussion in the preceding paragraphs shows that our Van Regemorter and CP cross sections are very useful in determining collisional excitation cross sections in realistic atomic and semiconductor systems. Given that experimental values of collisional excitation cross sections in quantum dots are not available now, the Van Regemorter and CP cross sections are perhaps the simplest, numerically reliable method at present.

Figures 4 and 5 show the collisional excitation cross section as a function of incident electron energy at room temperature for the $1S_{1/2}$-$1P_{1/2}$ transition in the conduction band of a 150-Å-radius InSb quantum dot surrounded by CdTe barriers. (The energy levels, symmetries, and notation for the bound states of this quantum dot have appeared elsewhere[18] in the literature. These and other relevant quantities are summarized in Table I.) These cross sections for our quantum dot could not be checked with experimental data, as no such data exists to the author's knowledge. To study our results, we will compare the cross sections obtained from both the CP methods in Figs. 4 and 5 with our VR cross section.

The weak (CPW) and intermediate (CPF,CPT) forms of the CP method in Fig. 4, obtained from (C6), (C14), and (C15) [with (C7) calculated to be $0.6R$], were obtained using the correct dielectric everywhere: $\epsilon=\epsilon_{\rm QD}$ when the incident particle is inside the quantum dot and $\epsilon=\epsilon_{ce}$ otherwise. The contribution from impact parameters greater than R, labeled $R>RQD$, is seen to be much smaller than the other CP cross sections in Fig. 4. Thus, the largest contributions to collisional excitation are from near collisions. The difference in the heights of the CPW, CPT, and CPF curves in Fig. 4 is a rough estimate of the errors incurred in estimating the contributions of the very near collisions using varying forms of the CP method. (See Appendix C.)

Since the quantum-dot collisional excitation cross section is dominated by the near collisions, specifically those which penetrate the quantum dot, we expect the difference in the quantum dot and barrier dielectric constants to be important for determining the collisional excitation cross section. The neglect of the difference in dielectric between the quantum dot and barrier materials makes the VR cross section, obtained from (4) and (7), much larger than the CP cross sections in Fig. 4. The Van Regemorter cross section of Figs. 4 and 5 uses $\epsilon=\epsilon_{ce}$ everywhere along the incident particle trajectory and is very similar to the classical path curve labeled CPF1 in

TABLE I. Intraband oscillator strengths and collisional excitation rate coefficients at room temperature for a 150-Å-radius InSb quantum dot surrounded by CdTe barriers. The bound state energies (measured from the bulk valence band edge) and symmetries have been discussed (Ref. 18) elsewhere. The intraband dipoles were checked by comparison with the analytical expressions given in Appendix A.

Electron state	Electron state	Electron energy (meV)	Oscillator strength $\sum_{F_{iz},F'_{iz}} f$	Collisional excitation rate coefficient q_{ij}^c (10^{-9} cm^3/s)
$1S_{1/2}$	$1P_{1/2}$	300	25.00	0.8054
(244 meV)	$1P_{3/2}$	300	32.95	1.062
(intraband)	$2P_{1/2}$	446	0.78	8.443×10^{-6}
	$2P_{3/2}$	446	1.09	1.180×10^{-5}

Fig. 5, which also uses $\epsilon=\epsilon_{ce}$ for all incident particle paths. Both the VR and CPF1 curves are noticeably different from the CPF curve of Fig. 5, which is the correct curve calculated using the correct dielectric everywhere.

The curve labeled CPF2 in Fig. 5 is calculated from the CP method (75) with $\epsilon=\epsilon_{ce}$ for those incident particle paths with the impact parameter greater than R, and $\epsilon=\epsilon_{\rm QD}$ *everywhere along* those incident particle paths with impact parameter less than R. CPF and CPF2 are similar because the dominant contribution to the cross section when the impact parameter is less than R occurs when the incident particle is inside the quantum dot.

Observe also that the typical quantum-dot collisional excitation cross section shown in Fig. 5 is much smaller than the physical size πR^2. This is in sharp contrast to the typical collisional excitation cross sections, which are roughly comparable to the physical size, either πa_0^2 or $\pi a_{\rm ex}^2$, in Figs. 2 and 3 for the hydrogen atom and the bulk exciton. The small size of the typical quantum-dot collisional excitation cross section is a result of the fact that E_{ji} is much larger than the Coulomb energy $(e^2/4\pi\epsilon_{ce}R)$ in (4) and (64), as we now show.

More specifically, we can understand the small size of the quantum-dot collisional excitation cross section relative to the physical size πR^2 by comparing (4) and (19),

$$\frac{Q_{\rm QD}^{\rm PEAK}(1S_{1/2}\text{-}1P_{1/2})}{Q_{H\text{ or ex}}^{PEAK}(1s\text{-}1p)} \sim \left[\left[\frac{e^2}{2\times4\pi\epsilon_{ce}R}\frac{1}{E_{ji}}\right]^2\pi R^2\right] \times\left[\left[\frac{I}{E_{ji}}\right]^2\pi a^2\right]_{H\text{ or ex}}^{-1}. \quad (23)$$

Equation (23) is obtained by noting that the scaled oscillator strength $(m_i/m_0)(\sum_{i,j}f_{ji}/3g_i)$ is roughly the same for most dipole allowed transitions: it is 0.416 for the $1s$-$2p$ transition in both the hydrogen atom and the exciton and it is $(m_i/m_0)(\sum_{i,j}f_{ji}/3g_i)=0.014\times25.00=0.35$ for the $1S_{1/2}$-$1P_{1/2}$ quantum-dot transition. Since the Gaunt factor is a function of $E_{\rm inc}/E_{ji}$, then $(E_{ji}/E_{\rm inc})g_G$ always has the same peak value. Whence, (23) follows.

Observe from (23) that the peak cross section for collisional excitation in hydrogen, in an exciton, and in a quantum dot is roughly equal to a geometric area (either πa^2 or πR^2) times the square of the ratio of a Coulomb energy to the collisional excitation energy. If we approximate $Q_{H\text{ or ex}}^{\rm PEAK}$ as πa_0^2 or $\pi a_{\rm ex}^2$, then $Q_{\rm QD}^{\rm PEAK}(1S_{1/2}\text{-}1P_{1/2})$ evaluates to $2.5\times10^{-3}\pi R^2$, in good agreement with Fig. 5.

For the $1s$-$2p$ transition in both the hydrogen atom and the exciton, $(I/E_{ji})^2=(\frac{4}{3})^2$, thus indicating that the typical bound state energy separation is about the same size as the typical Coulomb energy. For the $1S_{1/2}$-$1P_{1/2}$ quantum-dot transition, the analogous quantity is $[(e^2/2\times4\pi\epsilon_{ce}R)(1/E_{ji})]^2=4.5\times10^{-3}$. In other words, this small quantum dot has a typical Coulomb energy, which is inversely proportional to the radius, much smaller than the typical quantum confinement energy E_{ji},

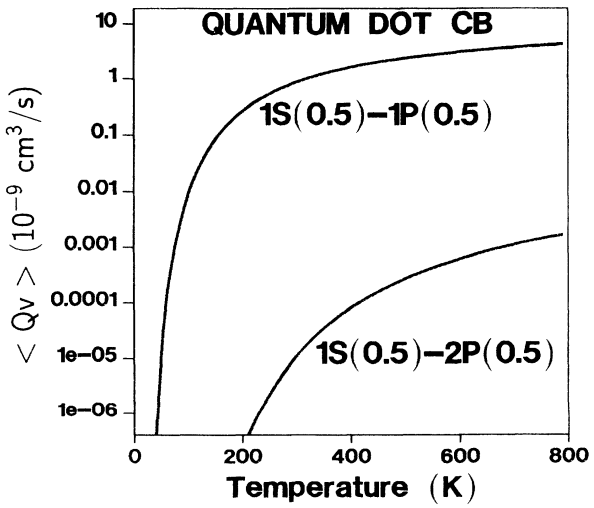

FIG. 6. The collisional excitation rate coefficients $q_{ij}^c=\langle Q_v\rangle$ (units of 10^{-9} cm^3/s) as a function of incident electron temperature for the $1S_{1/2}$-$1P_{1/2}$ ($E_{ji}=56$ meV) and $1S_{1/2}$-$2P_{1/2}$ ($E_{ji}=202$ meV) transitions in the conduction band of a 150-Å-radius InSb quantum dot surrounded by CdTe barriers. These rate coefficients were obtained by integrating the Van Regemorter cross sections over a Maxwellian distribution of incident free electrons, as in Eq. (12).

which is inversely proportional to the square of the radius. Unlike the hydrogen atom and the bulk exciton, this quantum confinement energy E_{ji} comes from the confining effects of the barrier material surrounding the quantum dot and is not the result of the Coulomb attraction between the bound electron and a proton (or hole). The small size of the typical quantum-dot collisional excitation cross section relative to its physical size πR^2 is thus a result of the large size of E_{ji} compared to the typical Coulomb energy $(e^2/4\pi\epsilon_{ce}R)$.

The collisional excitation rate coefficients $q_{ij}^c = \langle Q_v \rangle$ of Eq. (12) are shown in Fig. 6 as a function of incident electron temperature for the $1S_{1/2}$-$1P_{1/2}$ ($E_{ji}=56$ meV) and $1S_{1/2}$-$2P_{1/2}$ ($E_{ji}=202$ meV) transitions in the conduction band of our 150-Å-radius InSb quantum dot surrounded by CdTe barriers. As expected, the larger rate coefficients are associated with the smaller collisional energy exchange. The temperature dependences shown in Fig. 6 arise mainly from the occupation statistics of the incident electrons.

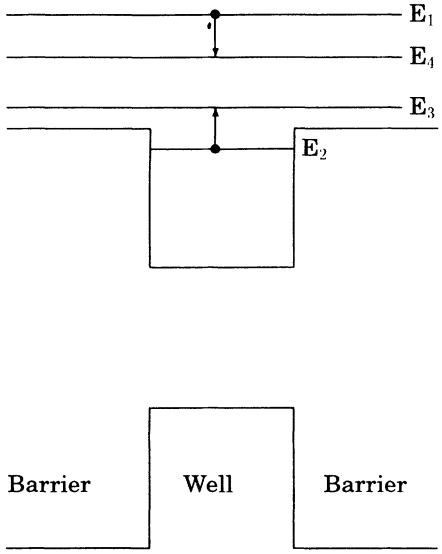

FIG. 7. In collisional ionization processes, the incident particle loses an energy $E_{32}=E_{14}$ of at least U_2 (the ionization potential of the bound particle) as it excites, via the Coulomb interaction between the two charged particles, a particle in the quantum dot from the bound state 2 to the continuum.

III. COLLISIONAL IONIZATION

Collisional ionization and its inverse, three-body recombination, can be indicated by the forward and reverse reactions, respectively,

$$X(Z-1,i)+e \rightleftharpoons X(Z)+e+e \ , \tag{24}$$

for an incident electron and for i in the conduction band. A similar equation can be written for incident holes and/or for i in the valence band. For the dominant collisional ionization processes, the bound (and the incident) particles make intraband transitions, for reasons discussed in Appendix A. In collisional ionization processes, the incident particle loses an energy of at least U_i (the ionization potential of the bound particle) as it excites, via the Coulomb interaction between the two charged particles, a particle in the quantum dot from the bound state i to the continuum, as shown in Fig. 7.

If we define $N(Z-1,i)$ as the population of the quantum dots $X(Z-1,i)$ and $N(Z)$ as the population of the parent "ion" $X(Z)$, then the collisional ionization rate out of and the three-body recombination rate into state i are, respectively, $N(Z-1,i)n_f q_i^{fb}$ and $N(Z)n_f n_b \alpha_3^{fb}(i)$, where $f=c,v$ denotes the energy band (conduction or valence) containing the incident free particle, $b=c,v$ denotes the energy band containing the bound state i, and n_f, n_b denote free carrier concentrations. The principle of detailed balance relates the coefficient for collisional ionization to that for three-body recombination,

$$\frac{q_i^{fb}}{\alpha_3^{fb}(i)} = \frac{g(Z)}{g(Z-1,i)} N_{b=c,v} \exp\left[\frac{-U(Z-1,i)}{k_B T}\right] , \tag{25}$$

where $U(Z-1,i)$ is the ionization potential of the quantum dot with total charge $Z-1$ and a particle in state i, and $g(Z)$ and $g(Z-1,i)$ are the statistical degeneracies of the initial and final quantum dot "ions."

In this section, we will present collisional ionization cross sections obtained from the binary encounter model. Our purpose is to show that the binary encounter model is very simple to use and of reliable numerical accuracy. Calculations based on the binary encounter model are in good agreement with experimentally inferred collisional ionization cross sections for the hydrogen atom and bulk excitons. Further, the simple analytical form of the binary cross sections yields physical insight into the study of collisional ionization from quantum dots, for which experimental data are not available.

Before presenting the binary encounter (BE) model, we report that we were not able to find an *ab initio* calculation of the collisional ionization cross section in bulk excitons. In the analysis of experimental data in low temperature, high field luminescence and conductivity studies of the collisional ionization of excitons, the collisional ionization cross section is often *assumed*[40–42] to be the geometric area πa_{ex}^2, where a_{ex} is the exciton Bohr radius. This is the curve labeled N in Fig. 8. The calculations based on this assumed cross section are usually within an order of magnitude of measured data: the Yao *et al.*[41] data were within a factor of 7 and Yamashita's[42] data were within an order of magnitude, with the best agreement being a factor of 2. More recently, agreement within a factor of 4 between the measured data and calculations based on the assumed cross section labeled N in Fig. 8 was reported by Nöldeke *et al.*[40]

Figure 8 shows that our BE cross sections for free carriers having energies above threshold are within an order of magnitude of the geometric area πa_{ex}^2 and are thus consistent with experimental measurements.

The use of the binary encounter model also provides insight not immediately available from the *ad hoc* assumption of a cross section equal to the geometric area πa_{ex}^2. For example, we find the curious result that the typical quantum-dot collisional ionization cross section is

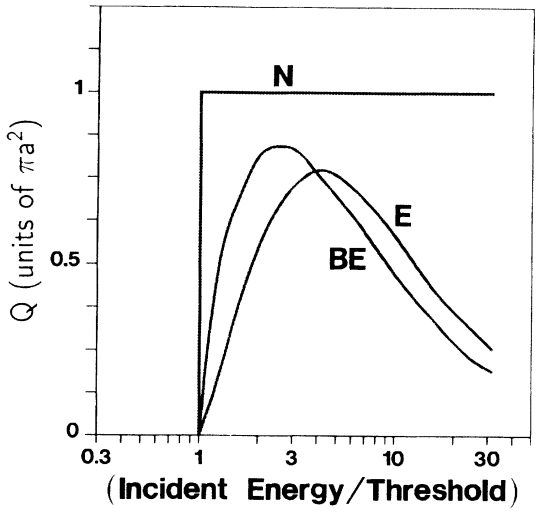

FIG. 8. The dependence on incident electron energy of the total collisional ionization cross section of hydrogen and of an exciton (with $m_e \ll m_h$) in a semiconductor. If the cross section is expressed in units of πa^2, where a is the Bohr radius for the hydrogen ionization problem and a is the exciton Bohr radius for the exciton ionization problem, and if the incident energy is expressed in units of the threshold (either the hydrogen or the exciton ionization potential), then the binary encounter collisional ionization cross section given by Eq. (26), is the curve (Ref. 43) labeled BE for ionization of both hydrogen and excitons. The experimental data (Ref. 43) labeled E are measurements made for hydrogen. The curve labeled N is the cross section often assumed (Refs. 40–42) in the analysis of experimental data from low temperature, high field studies of the collisional ionization of excitons. The calculations based on this assumed cross section were within a factor of 4 of the measured data of Nöldeke *et al.* (Ref. 40).

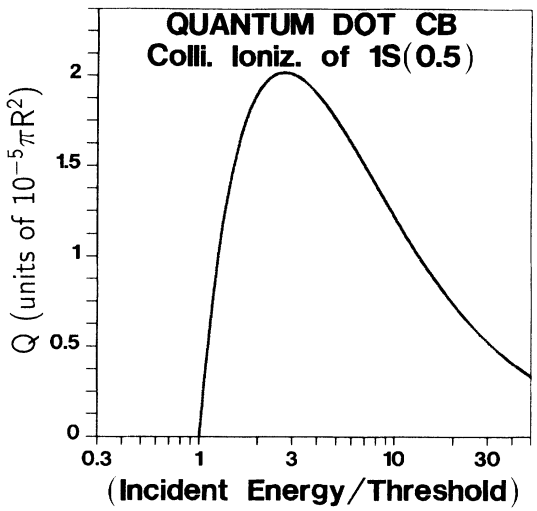

FIG. 9. The dependence on incident electron energy of the collisional ionization cross section (26), in units of $10^{-5}\pi R^2$, of the $1S_{1/2}$ ($U_i = 339$ meV) state in the conduction band of a 150-Å-radius InSb quantum dot surrounded by CdTe barriers.

much smaller than the physical size πR^2. The *ad hoc* assumption of a cross section equal to the geometric area πa_{ex}^2 does not allow one to understand this. As in the discussion of collisional excitation above, we will show in this section that the collisional ionization cross sections in quantum dots are much smaller than the physical size πR^2 because the typical Coulomb energy involved in the collision is much smaller than the typical ionization potential.

We emphasize that the power of the binary encounter model lies both in its simplicity and in its ability to provide numerics of comparable accuracy to what is now being used in studying bulk excitons. This success of the binary encounter model allows us to predict, as in Fig. 9, quantum-dot collisional ionization cross sections, for which experimental data is not yet available. We also calculate in Fig. 10 rate coefficients for the collisional ionization out of a bound state in an InSb quantum dot.

In Sec. III A, we present formulas for cross sections and rate coefficients in the binary encounter model of collisional ionization. In Sec. III B, we show that calculations based on this binary encounter model are in good agreement with experimental results for collisional ionization in atomic hydrogen (Fig. 8) and for excitons in bulk semiconductors. Figure 8 presents the first application of this simple model to the collisional ionization of excitons in a bulk semiconductor.

A. Binary encounter model

To calculate collisional ionization rates, we use a binary encounter[43–46] approximation, of which a very good review has been given by Vriens.[43] Hansen[46] has formulated the binary encounter approximation in spatial

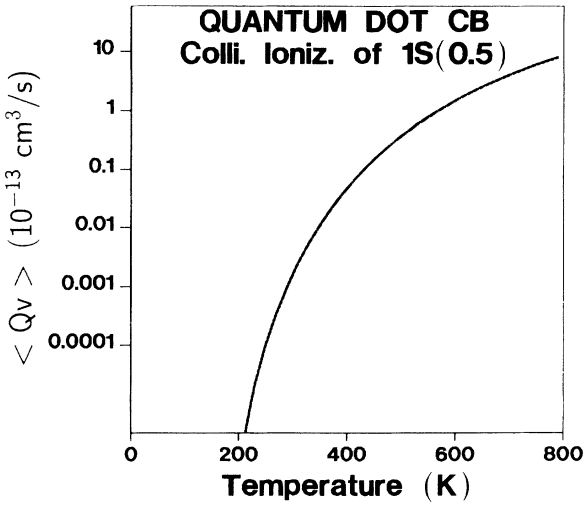

FIG. 10. The collisional ionization rate coefficient $q_i^{cc} = \langle Q_V \rangle$ (units of 10^{-13} cm^3/s) as a function of incident electron temperature for the $1S_{1/2}$ ($U_i = 339$ meV) state in the conduction band of a 150-Å-radius InSb quantum dot surrounded by CdTe barriers. This rate coefficient is obtained by integrating the binary encounter cross section (26) over a Maxwellian distribution of incident free electrons, as in Eq. (29).

coordinates so as to resemble the impact parameter method. This method has been used in realistic[13,45,46] descriptions of the collisional ionization processes in laboratory and astrophysical plasmas. The binary encounter model is known to give an accurate description of collisional ionization resulting from the near collisions of an incident particle with an atom or ion.

In the binary encounter model, the incident and the bound particles are modeled as free particles, of which the latter (the bound particle) has a velocity distribution appropriate for its bound state in the quantum dot. The cross sections for the Coulomb scattering of the two charged, moving, nonidentical particles are the same classically as quantum mechanically. For identical particles, the only modifications to the cross sections come from the interference between the direct and exchange terms.

The binary encounter model assumes that the incident particle interacts with only one bound (target) particle at a time. This assumption of the target particles as independent scattering centers would be justified when the interaction of the incident particle with the target particle takes place over spatial dimensions much smaller than the typical dimensions of the quantum dot. Consistent with this model is that the momentum (energy) transferred to the bound particle is large compared to the momentum (binding energy) of the bound particle before the collision.

In applying the Coulomb cross section to the collisional ionization of an electron by an incident electron, we use the symmetrized binary encounter model of Thomas and Burgess as described by Vriens.[43,44] We define $E_1 \equiv \frac{1}{2}m^* v_1^2$ as the incident particle energy (measured from the quantum barrier band edge), $E_2 \equiv \frac{1}{2}m^* v_2^2$ as the bound particle energy (measured from the quantum-dot band edge), and $U_i \equiv V_B - E_2$ as the ionization potential of (the bound) particle number 2. In this symmetrized model, we take the kinetic energy of the incident particle to increase to $E_1 + V_B$ (as compared to its kinetic energy of E_1 very far from the quantum dot) while the potential energy is taken as 0 (as compared to its potential energy of V_B very far from the quantum dot) during the interaction time of the classical encounter of the two particles.

In using the symmetrized binary encounter model for collisional ionization out of a quantum-dot bound state, we propose to use the quantum dot (and not the barrier) dielectric constant ϵ_{QD} as the relevant dielectric constant for the Coulomb interaction, as in (26). We do so because this would be consistent with the assumption of a near collision between the incident particle and the quantum dot. This value of the dielectric constant is also consistent with the discussion of the preceding paragraph of the incident particle kinetic and potential energies used in this model during the interaction time of the classical encounter.

1. Binary encounter cross section

The collisional ionization cross section in this symmetrized boundary encounter model is[43,44]

$$Q_i = \left[\frac{e^2}{4\pi\epsilon_{QD}}\right]^2 \left[\frac{\pi}{E_1+U_i+E_2}\right] \times \left[\left[\frac{1}{U_i}-\frac{1}{E_1}\right]+\frac{2}{3}E_2\left[\frac{1}{U_i^2}-\frac{1}{E_1^2}\right] - \frac{\Phi'}{E_1+U_i}\ln\left|\frac{E_1}{U_i}\right|\right], \tag{26}$$

where

$$\Phi' = \cos\left[\left[\frac{I^*}{E_1+U_i}\right]^{1/2}\ln\left|\frac{E_1}{U_i}\right|\right] \simeq 1 \tag{27}$$

because the energies

$$I^* = \frac{m^*}{2\hbar^2}\left[\frac{e^2}{4\pi\epsilon_{QD}}\right]^2 = \begin{cases} 0.61\text{meV} & \text{for electrons} \\ 0.65\text{meV} & \text{for light holes} \\ 17.43\text{meV} & \text{for heavy holes} \end{cases} \tag{28}$$

are small (for $\epsilon_{QD}=17.7$, $m_c=0.014m_0$, $m_{LH}=0.015m_0$, and $m_{HH}=0.4m_0$ in InSb) compared to the ionization energies U_i. (For InSb surrounded by CdTe, the barrier heights are 420 meV and 850 meV in the conduction and valence bands, respectively.) Equation (26) also assumes that there is no predetermined orientation between the velocities of the incident and bound particles; in other words, the bound particles have velocities of magnitude v_2 and of isotropic directional distribution.

2. Binary encounter rate coefficient

The collisional ionization rate of an electron by an incident electron is, using (26),

$$n_c q_i^{cc} \equiv n_c \langle Q_i v \rangle = n_c \left[\frac{e^2}{4\pi\epsilon_{QD}R}\right]^2 \left[\frac{v_{th,C}R^2}{4\pi^{5/2}(k_BT)^2}\right] P_{BE}\left[\frac{U_i}{k_BT}, \frac{E_2}{k_BT}\right], \tag{29}$$

where

$$P_{BE}\left[u_i=\frac{U_i}{k_BT}, \mathcal{E}_2=\frac{E_2}{k_BT}\right] = \int_{u_i}^{\infty}\frac{\mathcal{E}_1 d\mathcal{E}_1 \exp(-\mathcal{E}_1)}{\mathcal{E}_1+u_i+\mathcal{E}_2}\left[\left[\frac{1}{u_i}-\frac{1}{\mathcal{E}_1}\right]+\frac{2}{3}\mathcal{E}_2\left[\frac{1}{u_i^2}-\frac{1}{\mathcal{E}_1^2}\right]-\frac{1}{\mathcal{E}_1+u_i}\ln\left|\frac{\mathcal{E}_1}{u_i}\right|\right] \tag{30}$$

with $\mathcal{E}_1=E_1/k_BT$, $u_i=U_i/k_BT$, and $\mathcal{E}_2=E_2/k_BT$. This integral and its limiting forms are evaluated in Appendix D.

B. Numerical evaluation

In this subsection, we use our binary encounter formulas to calculate cross sections and rate coefficients for collisional ionization by electron impact in an hydrogen atom, in an exciton in a semiconductor, and in a quantum dot. As with our discussion of collision excitation in Sec. II C, we would like to demonstrate that this very simple model contains enough information to provide reliable numerics. First, we will review experimental measurements of the collisional ionization of hydrogen and compare these with results of the binary encounter model. Next, we present the first application of this simple model to the collisional ionization of excitons in semiconductors, and compare these results with experiment. Finally, we apply our model to the collisional ionization from quantum-dot bound states, for which our purpose is to estimate rate coefficients.

1. Calculations for hydrogen

The curve labeled BE in Fig. 8 shows the total collisional ionization cross section (where a is the Bohr radius for the hydrogen atom and the threshold is the hydrogen ionization potential) of hydrogen as a function of incident electron energy obtained from the symmetrized binary[43] encounter model, Eq. (26). The experimental data[43] labeled E are measurements made for hydrogen. Considering the great simplicity of the binary encounter model, this agreement with experiment is good. As in a similar discussion for collisional excitation in Sec. II C, the typical collisional ionization cross sections for both the hydrogen atom and the bulk exciton shown in Fig. 8 are comparable to the physical sizes πa_0^2 and $\pi a_{\rm ex}^2$, respectively.

2. Calculations for excitons

If the cross sections in Fig. 8 are expressed in units of πa^2, where a is the exciton Bohr radius, and if the incident energy is expressed in units of the exciton ionization potential, then the binary encounter collisional ionization cross section of an exciton with $m_c \ll m_h$ is also given by the curve[43] labeled BE [Eq. (26)]. We now show that this BE collisional ionization cross section is in reasonable agreement with experiment.

In the introduction to this section, we saw that in the analysis of experimental data in low temperature, high field luminescence and conductivity studies of bulk excitons, the collisional ionization cross section is often assumed[40–42] to be the geometric area $\pi a_{\rm ex}^2$. This is the curve labeled N in Fig. 8. The careful work of Nöldeke *et al.*,[40] Yao *et al.*,[41] and Yamashita[42] showed that calculations based on this assumed cross section are within an order of magnitude of the measured data. Figure 8 shows that our BE cross sections for free carriers having energies above threshold are within an order of magnitude of the geometric area $\pi a_{\rm ex}^2$ and are thus consistent with experimental measurements.

3. Calculations for quantum dots

The discussion in the preceding paragraphs shows that our BE cross section is useful in determining collisional ionization cross sections in realistic atomic or semiconductor systems. Given that experimental values of collisional ionization cross sections in quantum dots are not available now, the binary encounter cross section is perhaps the simplest, numerically reliable method at present. Figure 9 shows the collisional cross section (26), in units of $10^{-5}\pi R^2$, as a function of incident electron energy, of the $1S_{1/2}$ ($U_i=339$ meV) state in the conduction band of an 150-Å-radius InSb quantum dot surrounded by CdTe barriers. We have used the fact that $U_i \equiv V_B - E_2$.

As in Sec. II C, we have th curious fact that the typical quantum-dot collisional ionization cross section shown in Fig. 9 is much smaller than the physical size πR^2. Using Eq. (26), we can get the rough relationship for the peak collisional ionization cross section of $\sim[(e^2/2\times 4\pi\epsilon_{\rm QD}R)(1/U_i)]^2\pi R^2 = 6.4\times 10^{-5}\pi R^2$ in a quantum dot and $\sim(I/U_i)^2\pi a^2 \sim \pi a^2$ for the hydrogen atom (or exciton). Thus, the typical collisional ionization cross section of hydrogen (or an exciton) is comparable to the physical size πa^2 because the typical Coulomb energy $I_{H \text{ or ex}}$ is comparable to the typical ionization potential U. This makes sense since it is the Coulomb attraction which binds the electron to the positively charged proton (or hole).

For the quantum dot, the typical Coulomb energy $e^2/(2\times 4\pi\epsilon_{\rm QD}R)$ is much smaller than the typical ionization potential U and this allows the collisional ionization cross section to be much smaller than the physical size πR^2. The typical Coulomb energy is very different from the ionization potential for the quantum dot because it is the materials properties of the barrier material (and not the Coulomb potential of a hole or H nucleus) which binds the electron to the quantum dot.

Figure 10 shows the collisional ionization rate coefficient $q_i^{cc}=\langle Q_V \rangle$ (units of 10^{-13} cm^3/s), Eq. (29), as a function of incident electron temperature for the $1S_{1/2}$ ($U_i=339$ meV) state in the conduction band of 150-Å-radius InSb quantum dot surrounded by CdTe barriers. The temperature dependences shown in Fig. 10 arise mainly from the (Maxwellian) occupation statistics of the incident electrons.

A comparison of the cross sections in Figs. 5 and 9 can be used in conjunction with the rate coefficients in Fig. 6 to check the order of magnitude of the rate coefficients given in Fig. 10. We see that the typical collisional ionization cross section in Fig. 9 is about 10^{-2} times smaller than the typical collisional excitation cross section in Fig. 5. Upon integrating these cross sections over a Maxwellian distribution of free carriers, we expect a further reduction of a factor of $\exp[(56.1-339)/25.875] = 1.78\times 10^{-5}$ at room temperature as a result of the very different threshold energies for the collisional excitation $E_{ji}=56.1$ meV and the collisional ionization $U_i=339$

meV. Using the room-temperature collisional excitation rate coefficient given by the upper curve in Fig. 6, we estimate that the room-temperature collisional ionization rate coefficient for the $1S_{1/2}$ state is about $10^{-2}\times 1.78\times 10^{-5}\times 10^{-9}$ cm^3 s^{-1} $=1.78\times 10^{16}$ cm^3 s^{-1}, in good agreement with Fig. 10.

In the collisional ionization of holes, Eq. (26) must be modified to include an integration over the correct hole velocity distribution. The mixing[10,47] of the light and heavy hole eigenstates means that the correct hole velocity distribution at a particular eigenenergy must contain some component proportional to the heavy hole wave vector and some to the much smaller light hole wave vector. This is a subject for future work. For now, we note that in the InSb/CdTe system, the valence band potential barrier (850 meV) is much larger than the conduction band potential barrier (420 meV), and (80) gives a rough indication of how much smaller the hole ionization rates could be. Collisional ionization of electrons by incident holes can be studied using the formalism given by Vriens[43] for the incidence of heavy particles. For now, we note that as a result of the much larger valence band potential barrier in the InSb/CdTE system, the concentration of free holes n_v will be much smaller than that of the free electrons n_c, if the free carriers have a Maxwellian distribution as discussed in a future[15] work. Thus, the collisional ionization rate of bound electrons by incident electrons considered above should be the largest collisional ionization rate.

IV. CONCLUSIONS

We have applied to quantum dots formulas from atomic physics for collisional ionization (binary encounter model) and dipole allowed collisional excitation (Van Regemorter and classical path methods) rates. Given that experimental values of collisional cross sections in quantum dots are not available now, our methods are perhaps the simplest numerically reliable ones at present. The Van Regemorter, classical path, and binary encounter cross sections, which are known to be very successful in modeling atomic collisions, were shown to have accuracies comparable to (and are much easier to use than) the methods currently being used to study collisional rates in bulk excitons.

Collisional excitation and ionization cross sections for a 150-Å-radius InSb quantum dot surrounded by CdTe barriers were shown to be much smaller than the geometric area πR^2. The reason that these cross sections are so small is that the Coulomb energy associated with the collision is typically much smaller than the collisional energy exchange. When bound quantum-dot carriers cannot interact with phonons, the collisional processes discussed in this paper could make significant contributions to the ionization balance in semiconductor quantum dots.

Explicit formulas were given for quantum-dot intraband oscillator strengths.

ACKNOWLEDGMENT

J.L.P. thanks the AT&T Foundation and Rockwell International for financial support.

APPENDIX A: QUANTUM-DOT OPTICAL DIPOLES

In the $\mathbf{k}\cdot\mathbf{p}$ theory[48] of the allowed energy bands in the presence of a periodic potential, the electronic wave function is a product of a Bloch part, which is defined within the unit cell only, and an envelope part, which is defined at the lattice sites only. The physical significance of the wave vector associated with the envelope part is the translational symmetry of the bulk lattice. In many materials, the energy bands in reciprocal space can be approximted as having spherical symmetry. In such materials, it is possible to write all wave functions[47,10] as eigenstates of the total angular momentum. The total single particle angular momentum is the vector sum of the electron spin, the microscopic or Bloch angular momentum, and the envelope angular momentum.

The effect of an external potential whose typical range of interaction is many unit cells can be expressed as an effective Schrödinger equation acting on the envelope part of the wave function. For our quantum dots, the envelope wave functions "see" the potential formed by the barrier material to be rotationally symmetic. Boundary conditions are satisfied[47,10] by choosing the particle wave functions to be total angular momentum eigenstates. Quantum-dot eigenstates are thus of the form[10,47]

$$\Phi(\tau)=C_1\langle\sigma\Omega r|J=\tfrac{1}{2},L=F\pm\tfrac{1}{2};K\rangle_C+C_2\langle\sigma\Omega r|J=\tfrac{3}{2},L=F\mp\tfrac{1}{2};K\rangle$$
$$+C_3\langle\sigma\Omega r|j=\tfrac{3}{2},L=F\pm\tfrac{3}{2};K\rangle+C_4\langle\sigma\Omega r|J=\tfrac{1}{2},L=F\mp\tfrac{1}{2};K\rangle_S\ , \tag{A1}$$

where the C coefficients are obtained[18,47] by diagonalizing the $\mathbf{k}\cdot\mathbf{p}$ Hamiltonian and j denotes the quantum number associated with the vector sum of the spin and Bloch angular momenta,[47] L is the quantum number for the envelope angular momentum, F is the quantum number associated with the toal angular momentum, and K is the magnitude of the wave vector associated with the envelope function. For quantum dots surrounded by very large barriers, the electron wave functions can be approximated by the first term in (A1), whose radial component is proportional to a simple Bessel function. The literature[47] shows that the light and heavy hole bands in a semiconductor quantum dot mix significantly, so tht the bound hole states can be accurately approximated, to within an overall multiplicative normalization factor, as

$$\Phi_H(\tau)=[\langle\sigma\Omega|J=\tfrac{3}{2},L=L2\rangle(-b)j_{L3}(K_{\rm HH}R)\{j_{L2}(K_{\rm LH}R)j_{L2}(K_{\rm HH}r)-j_{L2}(K_{\rm HH}R)j_{L2}(K_{\rm LH}r)\}$$
$$+\langle\sigma\Omega|J=\tfrac{3}{2},L=L3\rangle(a+2)j_{L2}(K_{\rm HH}R)\{j_{L3}(K_{\rm LH}R)j_{L3}(K_{\rm HH}r)-j_{L3}(K_{\rm HH}R)j_{L3}(K_{\rm LH}r)\}]\ . \tag{A2}$$

The oscillator strength $f_{ji} \equiv (2m_0 E_{ji}/\hbar^2)|\langle i|\mathbf{r}|j\rangle|^2$ used in (4) is that appropriate for the collisionally excited *intraband* [both i and j must be in the same energy (conduction or valence) band] dipole transition between the bound states i,j. We neglect collisional processes involving an interband transition because the latter are much weaker than those involving only intraband transitions. There are two reasons for this. The first is that the Coulomb interaction acts on the envelope part rather than the lattice periodic Bloch part of the wave functions involved. (This fact is often used when calculating Auger rates[49,50] and bulk electron-electron, hole-hole, or electron-hole scattering[37] rates.) The remaining multiplicative factor in the matrix element (3) is the overlap integral between the initial and final lattice periodic Bloch functions, which is much smaller for an interband than for an intraband transition. (This overlap integral is identically zero for an interband transition involving a pure s type conduction band lattice periodic Bloch function and a pure p type valence band lattice periodic Bloch function. In this paper, we take this overlap integral to be unity for intraband transitions and zero for interband transitions.) The second reason is that collisional processes usually involve an energy exchange E_{ji} which is larger for an interband transition than for an intraband transition. We will see in Figs. 6 and Eqs. (B2) and (D2) that larger energy exchanges result in smaller collisional rates. Thus, in the dominant collisional processes, the bound (and the incident) particles make intraband transitions.

1. Radial envelope overlap integrals for interband dipole transitions

Optical dipoles for quantum-dot conduction to valence band transitions have already been calculated in the literature.[11,10] The dipole operator is taken between the s- and p-like cell-periodic Bloch functions. Since analytical expressions for the radial envelope overlap integrals were not presented in these papers, we list them below. We have checked that these analytical expressions agree with our previous[11] numerical results. Using the fact that

$$j_n(z) = \left[\frac{\pi}{2z}\right]^{1/2} J_{n+1/2}(z) \tag{A3}$$

and the integrals given in page 254 of Luke's book,[51] we have, for $k_1 \neq k_2$,

$$\int_0^R r^2 dr\, j_l(k_2 r) j_l(k_1 r) = \frac{R^2}{k_2^2 - k_1^2}\{k_2 j_{l+1}(k_2 R) j_l(k_1 R) - k_1 j_l(k_2 R) j_{l+1}(k_1 R)\} . \tag{A4}$$

Normalization integrals can also be calculated:

$$\begin{aligned}\int_0^R r^2 dr [j_m(kr)]^2 &= \frac{R^3}{2}\{j_m^2(kR) - j_{m-1}(kR) j_{m+1}(kR)\} \\ &= \frac{R^3}{2}\left\{j_m^2(kR) + j_{m+1}^2(kR) - \frac{2m+1}{kR} j_m(kR) j_{m+1}(kR)\right\} \\ &= \frac{R^3}{2}\left\{j_m^2(kR) + j_{m-1}^2(kR) - \frac{2m+1}{kR} j_m(kR) j_{m-1}(kR)\right\} .\end{aligned} \tag{A5}$$

When $j_m(kR)=0$, this becomes

$$\int_0^R r^2 dr [j_m(kr)]^2 = \frac{R^3}{2} j_{m+1}^2(kR) = \frac{R^3}{2} j_{m-1}^2(kR) . \tag{A6}$$

2. Dipoles for intraband transitions

Suppose we want to calculate the z component of the dipole,

$$z = r\left[\frac{4\pi}{3}\right]^{1/2} Y_{l=1,M=0} . \tag{A7}$$

In intraband transitions, the dipole operator acts on the envelope part of the particle wave functions. If we write r_M as the component of $\mathbf{r}$ proportional to the spherical harmonic $Y_{l=1,M}$, then, using the notation for the wave function given in the literature,[18,11]

$$\langle \Phi_i | r_M | \phi_{i'}' \rangle = \sum_{(J_i,L_i)} \sum_{(J_i',L_i')} C^*_{K,(L_{Bi},S_i)J_i,L_i} C_{K',(L_{Bi}',S_i')J_i',L_i'} \langle f_{L_i}|r|f_{L_i'}\rangle \left[\frac{4\pi}{3}\right]^{1/2} \langle J_i,L_i;F_i,F_{iz}|Y_{l=1,M}|J_i',L_i';F_i',F_{iz}'\rangle , \tag{A8}$$

where the C coefficients are obtained[18,47] by diagonalizing the $\mathbf{k}\cdot\mathbf{p}$ Hamiltonian. The angular factor is

$$\langle J_i,L_i;F_i,F_{iz}|Y_{l,M}|J_i',L_i';F_i',F_{iz}'\rangle=\delta_{F_{iz},M+F_{iz}'}\delta_{J_i,J_i'}\langle L_i\|l\|L_i'\rangle\langle l,M;F_i',F_{iz}'|l,F_i';F_i,F_{iz}\rangle$$
$$\times[(2F_i'+1)(2L_i+1)]^{1/2}W(lL_i'F_iJ_i;L_iF_i')(-1)^{3l-2L_i'+6J_i+F_i+F_i'}\ . \tag{A9}$$

3. Radial integrals for intraband electron transitions

We can differentiate (A4) with respect to the wave vector k_2 and use the recursion relation among Bessel functions and their derivatives to obtain

$$\int_0^R r^2dr\, j_m(k_1r)j_{m+1}(k_2r)r=\left[\frac{R^2}{k_1^2-k_2^2}\right]\left[j_{m+1}(k_1R)j_m(k_2R)\left\{\frac{-2k_1k_2}{k_1^2-k_2^2}\right\}\right.$$
$$+j_m(k_1R)j_{m+1}(k_2R)\left\{\frac{-2k_2^2}{k_1^2-k_2^2}-(2m+1)\right\}$$
$$\left.+(k_1R)j_{m+1}(k_1R)j_{m+1}(k_2R)+(k_2R)j_m(k_1R)j_m(k_2R)\right]\ . \tag{A10}$$

The selection rules enforced by the reduced matrix element in (A9) ensure that these are the only types of radial integrals to calculate. For the electron eigenstates in the conduction band of a quantum dot, we have, approximately,

$$j_m(k_1R)=j_{m+1}(k_2R)=0\ , \tag{A11}$$

from whence we have

$$\frac{\left|\int_0^R r^2dr j_m(k_1r)j_{m+1}(k_2r)r\right|}{\left[\int_0^R r_1^2dr_1j_m^2(k_1r_1)\int_0^R r_2^2dr_2j_{m+1}(k_2r_2)\right]^{1/2}}=R\frac{4(k_1R)(k_2R)}{|(k_1R)^2-(k_2R)^2|^2}\ . \tag{A12}$$

The reduced matrix element $\langle L\|l\|L'\rangle$ is defined[18,11,52] in the standard way. Using the fact that

$$\sum_{F_{iz},F_{iz}'}|\langle l,M;F_i',F_{iz}'|l,F_i';F_iF_{iz}\rangle|^2=\left[\frac{2F_i+1}{2l+1}\right]\ , \tag{A13}$$

and working out the angular factors in (A8) and (A9), we have, assuming that the conduction band wave functions have no valence band character,

$$\sum_{F_{iz},F_{iz}'}|\langle\Phi_i|\mathbf{r}|\Phi_{i'}'\rangle|^2=\begin{cases}R^2\dfrac{(K_iR)^2(K_i'R)^2}{|(K_iR)^2-(K_i'R)^2|^4}\left[\dfrac{4(2F_i+1)}{3(F_i+1)}\dfrac{1}{F_i}\right] & \text{for } F_i'=F_i\\ R^2\dfrac{(K_iR)^2(K_i'R)^2}{|(K_iR)^2-(K_i'R)^2|^4}\left[\dfrac{4(2F_i+1)}{3(F_i+1)}(2F_i+3)\right] & \text{for } F_i'=F_i+1\ .\end{cases} \tag{A14}$$

Upon further assuming that the bulk conduction band is perfectly parabolic with an effective mass of m_c, the oscillator strength is

$$|f_{i'i}|\equiv\frac{2m_0|F_{i'i}|}{\hbar^2}|\langle i|\mathbf{r}|i'\rangle|^2=\begin{cases}\dfrac{m_0}{m_c}\left[\dfrac{(K_iR)^2(K_i'R)^2}{|(K_iR)^2-(K_i'R)^2|^3}\right]\left[\dfrac{4(2F_i+1)}{3(F_i+1)}\dfrac{1}{F_i}\right] & \text{for } F_i'=F_i\\ \dfrac{m_0}{m_c}\left[\dfrac{(K_iR)^2(K_i'R)^2}{|(K_iR)^2-(K_i'R)^2|^3}\right]\left[\dfrac{4(2F_i+1)}{3(F_i+1)}(2F_i+3)\right] & \text{for } F_i'=F_i+1\ .\end{cases} \tag{A15}$$

The conduction band in small band gap semiconductors such as InSb could deviate very noticeably (see Fig. 1.20 of Ridley's[37] book) from a parabolic wave vector dispersion relation of effective mass m_c, and (A15) should be used with caution.

4. Radial integrals for bound-free intraband electron transitions

For bound-free electron intraband optical dipoles, we use (A5) and (A10) above, with (A11) applying for the bound state only. For quantum dots surrounded by large potential barriers, the wave vector of the free particle (while it is in the quantum dot) approximately satisfies $(kR)\gg 1$, so that the large argument asymptotic limit of the spherical Bessel function may be used,

$$j_m(z)\simeq\frac{\cos\left[z-(m+1)\frac{\pi}{2}\right]}{z}\quad |z|\gg 1\ . \tag{A16}$$

For

$$j_m(k_1R)=0\ ,\quad (k_2R)\gg 1\ , \tag{A17}$$

we have

$$\frac{\left|\int_0^R r^2 dr j_m(k_1r)j_{m+1}(k_2r)r\right|}{\left[\int_0^R r_1^2dr_1 j_m^2(k_1r_1)\int_0^R r_2^2dr_2 j_{m+1}(k_2r_2)\right]^{1/2}}=\frac{2R}{|(k_1R)^2-(k_2R)^2|}\times\left|\left\{\frac{-2(k_1R)(k_2R)}{(k_1R)^2-(k_2R)^2}\right\}\cos\left[k_2R-(m+1)\frac{\pi}{2}\right]+(k_1R)\cos\left[k_2R-(m+2)\frac{\pi}{2}\right]\right| \tag{A18}$$

and for

$$j_{m+1}(k_2R)=0\ ,\quad (k_1R)\gg 1\ , \tag{A19}$$

we have

$$\frac{\left|\int_0^R r^2 dr j_m(k_1r)j_{m+1}(k_2r)r\right|}{\left[\int_0^R r_1^2dr_1 j_m^2(k_1r_1)\int_0^R r_2^2dr_2 j_{m+1}(k_2r_2)\right]^{1/2}}=\frac{2R}{|(k_1R)^2-(k_2R)^2|}\times\left|\left\{\frac{-2(k_{1R})(k_2R)}{(k_1R)^2-(k_2R)^2}\right\}\cos\left[k_1R-(m+2)\frac{\pi}{2}\right]+(k_2R)\cos\left[k_1R-(m+1)\frac{\pi}{2}\right]\right|. \tag{A20}$$

Though (A20) is a convenient way to present the bound-free intraband dipole, it should be remembered that the free particle is normalized to L^3, the macroscopic volume of the sample, and not to the volume of the quantum dot as in (A20).

5. Radial integrals for intraband hole transitions

The mixing[47] of the light and heavy holes makes the expressions for intraband hole optical dipoles much more cumbersome than for intraband electron optical dipoles. These expressions are useful for checking numerical work in this area, and we present them for completeness. The normalization integrals are

$$\begin{aligned}&\int_0^R r^2dr[j_m(K_{\rm HH}R)j_m(K_{\rm LH}r)-j_m(K_{\rm LH}R)j_m(K_{\rm HH}r)]^2\\&=\frac{R^3}{2}j_m^2(K_{\rm HH}R)\left\{j_m^2(K_{\rm LH}R)+j_{m+1}^2(K_{\rm LH}R)-\frac{2m+1}{K_{\rm LH}R}j_m(K_{\rm LH}R)j_{m+1}(K_{\rm LH}R)\right\}\\&+\frac{R^3}{2}j_m^2(K_{\rm LH}R)\left\{j_m^2(K_{\rm HH}R)+j_{m+1}^2(K_{\rm HH}R)-\frac{2m+1}{K_{\rm HH}R}j_m(K_{\rm HH}R)j_{m+1}(K_{\rm HH}R)\right\}\\&-2j_m(K_{\rm HH}R)j_m(K_{\rm LH}R)\left[\frac{R^2}{K_{\rm LH}^2-K_{\rm HH}^2}\right]\{K_{\rm LH}j_{m+1}(K_{\rm LH}R)j_m(K_{\rm HH}R)-K_{\rm HH}j_m(K_{\rm LH}R)j_{m+1}(K_{\rm HH}R)\}\ .\end{aligned} \tag{A21}$$

The dipole is

$$
\begin{aligned}
&\int_0^R r^2 dr [j_m(K_{1HH}R)j_m(K_{1LH}r)-j_m(K_{1LH}R)j_m(K_{1HH}r)] \\
&\quad\times r[j_{m+1}(K_{2HH}R)j_{m+1}(K_{2LH}r)-j_{m+1}(K_{2LH}R)j_{m+1}(K_{2HH}r)] \\
&\quad= R^2\left[\left[\frac{j_m(K_{1HH}R)j_{m+1}(K_{2HH}R)}{K_{1LH}^2-K_{2LH}^2}\right]\left[j_{m+1}(K_{1LH}R)j_m(K_{2LH}R)\left\{\frac{-2K_{1LH}K_{2LH}}{K_{1LH}^2-K_{2LH}^2}\right\}\right.\right. \\
&\qquad\qquad +j_m(K_{1LH}R)j_{m+1}(K_{2LH}R)\left\{\frac{-2K_{2LH}^2}{K_{1LH}^2-K_{2LH}^2}-(2m+1)\right\} \\
&\qquad\qquad \left.+(K_{1LH}R)j_{m+1}(K_{1LH}R)j_{m+1}(K_{2LH}R)+(K_{2LH}R)j_m(K_{1LH}R)j_m(K_{2LH}R)\right] \\
&\qquad -\left[\frac{j_m(K_{1HH}R)j_{m+1}(K_{2LH}R)}{K_{1LH}^2-K_{2HH}^2}\right]\left[j_{m+1}(K_{1LH}R)j_m(K_{2HH}R)\left\{\frac{-2K_{1LH}K_{2HH}}{K_{1LH}^2-K_{2HH}^2}\right\}\right. \\
&\qquad\qquad +j_m(K_{1LH}R)j_{m+1}(K_{2HH}R)\left\{\frac{-2K_{2HH}^2}{K_{1LH}^2-K_{2HH}^2}-(2m+1)\right\} \\
&\qquad\qquad \left.+(K_{1LH}R)j_{m+1}(K_{1LH}R)j_{m+1}(K_{2HH}R)+(K_{2HH}R)j_m(K_{1LH}R)j_m(K_{2HH}R)\right] \\
&\qquad -\left[\frac{j_m(K_{1LH}R)j_{m+1}(K_{2HH}R)}{K_{1HH}^2-K_{2LH}^2}\right]\left[j_{m+1}(K_{1HH}R)j_m(K_{2LH}R)\left\{\frac{-2K_{1HH}K_{2LH}}{K_{1HH}^2-K_{2LH}^2}\right\}\right. \\
&\qquad\qquad +j_m(K_{1HH}R)j_{m+1}(K_{2LH}R)\left\{\frac{-2K_{2LH}^2}{K_{1HH}^2-K_{2LH}^2}-(2m+1)\right\} \\
&\qquad\qquad \left.+(K_{1HH}R)j_{m+1}(K_{1HH}R)j_{m+1}(K_{2LH}R)+(K_{2LH}R)j_m(K_{1HH}R)j_m(K_{2LH}R)\right] \\
&\qquad +\left[\frac{j_m(K_{1LH}R)j_{m+1}(K_{2LH}R)}{K_{1HH}^2-K_{2HH}^2}\right]\left[j_{m+1}(K_{1HH}R)j_m(K_{2HH}R)\left\{\frac{-2K_{1HH}K_{2HH}}{K_{1HH}^2-K_{2HH}^2}\right\}\right. \\
&\qquad\qquad +j_m(K_{1HH}R)j_{m+1}(K_{2HH}R)\left\{\frac{-2K_{2HH}^2}{K_{1HH}^2-K_{2HH}^2}-(2m+1)\right\} \\
&\qquad\qquad \left.\left.+(K_{1HH}R)j_{m+1}(K_{1HH}R)j_{m+1}(K_{2HH}R)+(K_{2HH}R)j_m(K_{1HH}R)j_m(K_{2HH}R)\right]\right] .
\end{aligned}
\tag{A22}
$$

APPENDIX B: THE VAN REGEMORTER $P_{VR}(E_{ji}/k_BT)$

The Van Regemorter $P_{VR}(E_{ji}/k_BT)$ integral is defined to be

$$
P_{VR}\left[\frac{E_{ji}}{k_BT}\right]=\int_{E_{ji}/k_BT}^{\infty} d\mathcal{E}\,\exp(-\mathcal{E})g_G(\mathcal{E}) , \tag{B1}
$$

where $\mathcal{E}=E_{inc}/k_BT$ and g_G is the Van Regemorter Gaunt factor (7). Using Eq. (7), this integral is evaluated to be

$$
\begin{aligned}
P_{VR}(\mathcal{E})=&\frac{\sqrt{3}}{2\pi}E_1([x_0^2+1]\mathcal{E})-\left[\frac{3}{2}\frac{0.051}{\mathcal{E}}\right]\exp(-2\mathcal{E}) \\
&+\frac{\exp(-\mathcal{E})}{\sqrt{\mathcal{E}}}\frac{\sqrt{\pi}}{2}\left[\operatorname{erf}(\sqrt{\mathcal{E}})\left\{0.073+\frac{3}{2}\frac{0.051}{\mathcal{E}}-\frac{1}{(x_0-1)}\left[\frac{\sqrt{3}}{2\pi}\ln|x_0^2+1|-0.124\right]\right\}\right. \\
&\left.+\operatorname{erf}(x_0\sqrt{\mathcal{E}})\frac{1}{(x_0-1)}\left[\frac{\sqrt{3}}{2\pi}\ln|x_0^2+1|-0.124\right]\right] ,
\end{aligned}
\tag{B2}
$$

where we will choose $x_0=4$ to match the large incident energy limit of the correct Gaunt factor, the error function is $\mathrm{erf}(x)=(2/\sqrt{\pi})\int_0^x \exp(-t^2)dt$, and the exponential integral is $E_1(x)=\int_x^\infty (dt/t)\exp(-t)$. The exponential integral[53] has the asymptotic forms

$$E_1(x)=\begin{cases} -0.57721-\ln x & \text{for } |x|\ll 1 \\ \dfrac{\exp(-x)}{x}\left[1-\dfrac{1}{x}+\dfrac{2}{x^2}\right] & \text{for } |x|\gg 1 \end{cases} . \tag{B3}$$

For very small E_{ji}/k_BT, $P_{\mathrm{VR}}(E_{ji}/k_BT)$ can be approximated as

$$P_{\mathrm{VR}}\left[\frac{E_{ji}}{k_BT}\right]\simeq\frac{\sqrt{3}}{2\pi}E_1\left[\frac{E_{ji}}{k_BT}\right] . \tag{B4}$$

APPENDIX C: THE CLASSICAL PATH METHOD

The details of Seaton's classical path model, which we now present, applies to scattering off a neutral target. Burgess and Summers[13] have generalized the classical path model to charged targets. A very good review of these semiclassical methods for calculating the collisional excitation cross sections, as well as a comparison of these with quantum mechanical results for all multipole orders, was discussed by Alder *et al.*[26] for nuclear scattering problems.

In the classical path method, we assume that the path of the incident particle can be described classically. For neutral targets, this incident particle's path $\mathbf{r}'(t)$ is a straight line whose closest approach to the quantum dot is the impact parameter R_i,

$$\mathbf{r}'(t)=R_i\hat{x}+(v_{\mathrm{inc}}t)\hat{y} , \tag{C1}$$

where the x-y plane contains both the quantum dot and the path of the incident particle and $\hat{y}$ is the direction of the velocity of the incident particle.

The probability of making a transition from the upper state j to the lower state i is

$$P_{ji}=\frac{1}{\hbar^2 g_j}\sum_{\text{degenerate } i,\text{degenerate } j}\left|\int_{-\infty}^{\infty}dt\,\exp\left[i\frac{E_{ji}}{\hbar}t\right]V_{ji}(t)\right|^2 , \tag{C2}$$

where g_j is the degeneracy of the initial state and $V_{ji}(t)$ is determined by (3) and (C1). The Coulomb interaction in (3) can be expanded in terms of multipole moments. Using the classical path in (C1), it is easy to show[25] that, for dipole allowed excitations,

$$P_{ji,CPW}(R_i)=\left[\frac{e^2}{4\pi\epsilon_{ce}R}\right]^2\left[\frac{m_i}{m_0}\right]\left[\frac{\sum f_{ji}}{3g_i}\right]\times\left[\frac{1}{E_{ji}E_{\mathrm{inc}}}\right]\left[\frac{R}{R_i}\right]^2\zeta(\beta_i) , \tag{C3}$$

where we use the symmetrized β parameter of Seaton,

$$\beta_i=\frac{R_iE_{ji}}{\hbar v_{\mathrm{inc}}}=\left[\frac{2m_i}{\hbar^2}E_{\mathrm{inc}}\right]^{1/2}R_i\left[\frac{E_{ji}}{2E_{\mathrm{inc}}-E_{ji}}\right] \tag{C4}$$

and the function

$$\zeta(\beta)=\beta^2[K_0^2(\beta)+K_1^2(\beta)] \tag{C5}$$

has been tabulated and approximated by Seaton. The $K_{0,1}(\beta)$ are Bessel functions. Our expression (C3) differs slightly from that of Seaton[25] in order to account for semiconductor materials parameters.

1. Weak coupling limit

When the states i and j have a relatively weak coupling (small oscillator strength), then the probability in (C3) is less than unity and we may integrate over all impact parameters greater than a certain cutoff parameter R_{co} to find the cross section

$$Q_{\mathrm{CPW}}(i\rightarrow j)=\int_{R_{\mathrm{co}}}^{\infty}P_{ji}(R_i)2\pi R_i dR_i . \tag{C6}$$

Physically, since the weak coupling limit of the CP model assumes that the incident particle does not penetrate the target, we choose R_{co} to be the physical size of the electron "orbits," which we take to be the geometric mean of the root mean square orbit size of the i,j states,

$$R_{\mathrm{co}}=[\langle i|r^2|i\rangle\langle j|r^2|j\rangle]^{1/4} . \tag{C7}$$

Numerically, this choice of R_{co} allows the CP cross sections to match the Bethe approximation as given by Van Regemorter[24] at large incident energies, as we would expect.[39]

In the weak coupling limit, we have

$$Q_{\mathrm{CPW}}(i\rightarrow j)=\left[\frac{m_i}{m_0}\right]\left[\frac{2\sum_{i,j}f_{ji}}{3g_i}\right]\left[\frac{1}{E_{ji}E_{\mathrm{inc}}}\right]\times\left[\frac{e^2}{4\pi\epsilon_{ce}R}\right]^2\phi(\beta_{\mathrm{co}})(\pi R^2) , \tag{C8}$$

where β_{co} is (C4) evaluated at the cutoff impact parameter R_{co} and the function

$$\phi(\beta_{\mathrm{co}})=\int_{\beta_{\mathrm{co}}}^{\infty}\frac{\zeta(\beta)}{\beta}d\beta=\beta_{\mathrm{co}}K_0(\beta_{\mathrm{co}})K_1(\beta_{\mathrm{co}}) \tag{C9}$$

has been tabulated by Seaton.[25] For small β_{co} (large incident energies),

$$\phi(\beta_{\mathrm{co}})\simeq\ln\left|\frac{1.1229}{\beta_{\mathrm{co}}}\right| , \tag{C10}$$

which is the Bethe limit.

2. Strong coupling limit

Both of the Van Regemorter and the classical path CPW cross sections are based on the Bethe[54] approximation, which is valid for incident particle energies much larger than the threshold energy. As such, the Bethe approximation accurately models the high incident energy,

distant encounters (those which do not penetrate the quantum dot or atom) of the incident particle. Near the threshold energy, the Bethe approximation fails, and both the Van Regemorter and classical path cross sections make allowances for this. Van Regemorter used an empirical Gaunt factor obtained from the best experimental data then available.

In the strong coupling limit, the dipole between states i and j is characterized by a large oscillator strength. This classical path model will still give reasonable answers if we limit the transition probabilities in (C3) to physically accessible values; i.e., P_{ji} must be less than unity. Seaton[25] accomplished this by choosing as the lower limit of the integration over impact parameter that value of impact parameter which allows the transition probability to be $\frac{1}{2}$. That is, we define R_1 from

$$P_{ji}(R_1)=\tfrac{1}{2} \tag{C11}$$

and integrate only over those impact parameters greater than R_1. For impact parameters less than R_1 (the near collisions), we would not use (C3), since it gives unphysical probabilities. Instead, for these impact parameters, we assume that the transition probabilities have an average value of $\frac{1}{2}$.

The cross section is then

$$Q_{\mathrm{CPS}}(i\rightarrow j)=\tfrac{1}{2}\pi R_1^2+\int_{R_1}^{\infty}P_{ji}(R_i)2\pi R_i dR_i \ . \tag{C12}$$

This evaluates to

$$Q_{\mathrm{CPS}}(i\rightarrow j)=\left[\frac{m_i}{m_0}\right]\left[\frac{2\sum_{i,j}f_{ji}}{3g_i}\right]\left[\frac{1}{E_{ji}E_{\mathrm{inc}}}\right]\left[\frac{e^2}{4\pi\epsilon_{ce}R}\right]^2 \times[\phi(\beta_1)+\tfrac{1}{2}\zeta(\beta_1)](\pi R^2) \ , \tag{C13}$$

where β_1 is (C4) evalautd at R_1. In practice, we choose the smaller of the two expressions (C8) and (C13) as the classical path cross section for the collisional excitation to a final state which is strongly dipole coupled to the initial state.

3. Intermediate coupling

Recently Hagelstein[39] has proposed a classical path model intermediate between the strong and weak coupling limits just discussed. In this intermediate form of the CP model, contributions to the collisional excitation cross section from those impact parameters less than R_{co} are not ignored as they are in the weak coupling limit (C6). However, transition probabilities for these near collisions cannot be taken, as in the strong coupling limit (67), to be $\frac{1}{2}$, which could result in cross sections much larger[39] than those observed, as in the case of highly stripped ions. Instead, the transition probabilities for small impact parameters are taken to be a constant (i.e., "flat") equal to its value at the cutoff radius R_{co},

$$P_{ji,\mathrm{CPF}}(R_i)=\begin{cases}P_{ji,\mathrm{CPW}}(R_i) & \text{for } R_i>R_{\mathrm{co}}\\ P_{ji,\mathrm{CPW}}(R_{\mathrm{co}}) & \text{for } R_i<R_{\mathrm{co}}\end{cases} \ . \tag{C14}$$

For large impact parameters, the transition probabilities are still taken as (C3). Hagelstein[39] further proposes that a better model for the near collisions would be to take the transition probability to be linear (i.e., "triangular") for small impact parameters,

$$P_{ji,\mathrm{CPT}}(R_i)=\begin{cases}P_{ji,\mathrm{CPW}}(R_i) & \text{for } R_i>R_{\mathrm{co}}\\ \dfrac{R_i}{R_{\mathrm{co}}}P_{ji,\mathrm{CPW}}(R_{\mathrm{co}}) & \text{for } R_i<R_{\mathrm{co}}\end{cases} \tag{C15}$$

and continues at the cutoff radius R_{co}. Good agreement[39] has been obtained between experiment and this intermediate form of the CP model for those ions[39] in which collisional excitation is dominated by near collisions.

The intermediate form of the CP model will be used in this paper to describe collisional excitation, which is seen to be dominated by near collisions, in quantum dots. The collisional excitation cross section obtained from (C14) is

$$Q_{\mathrm{CPF}}(i\rightarrow j)=\left[\frac{m_i}{m_0}\right]\left[\frac{2\sum_{i,j}f_{ji}}{3g_i}\right]\left[\frac{1}{E_{ji}E_{\mathrm{inc}}}\right]\left[\frac{e^2}{4\pi\epsilon_{ce}R}\right]^2 \times[\phi(\beta_{\mathrm{co}})+\tfrac{1}{2}\zeta(\beta_{\mathrm{co}})](\pi R^2) \ . \tag{C16}$$

The collisional excitation cross section obtained from (C15) is

$$Q_{\mathrm{CPT}}(i\rightarrow j)=\left[\frac{m_i}{m_0}\right]\left[\frac{2\sum_{i,j}f_{ji}}{3g_i}\right]\left[\frac{1}{E_{ji}E_{\mathrm{inc}}}\right]\left[\frac{e^2}{4\pi\epsilon_{ce}R}\right]^2 \times[\phi(\beta_{\mathrm{co}})+\tfrac{1}{3}\zeta(\beta_{\mathrm{co}})](\pi R^2) \ . \tag{C17}$$

4. Approximate adjustment for the quantum-dot dielectric

The classical path cross sections shown in Fig. 4 were calculated numerically with the correct dielectric everywhere: $\epsilon=\epsilon_{\mathrm{QD}}$ when the incident particle is inside the quantum dot and $\epsilon=\epsilon_{ce}$ otherwise. Use of the correct dielectric is important in obtaining the correct limiting forms for the collisional excitation cross section. At large incident energies, the cross section is dominated by the far collisions, for which the appropriate dielectric is ϵ_{ce} ($=12.7$ in the InSb/CdTe system), but at incident energies near threshold, the cross section is dominated by the near collisions, for which the appropriate dielectric is ϵ_{QD} ($=17.7$ in the InSb/CdTe system). In the equations above, we have not accounted for this difference in dielectrics, since we have assumed a dielectric of ϵ_{ce} everywhere, as in (C5), (C16), and (C17).

Though the use of the correct dielectric everywhere is the correct way to use the CP method, it is also unwieldy because it must be done numerically. We now propose a new version of Seaton's CP model which approximately accounts for the dielectric difference between the quantum dot and barrier, but which does not require a numerical integration. Our version of the CP model is based on the observation that when the impact parameter is less

than the quantum-dot radius, the dominant contribution to the CP cross section occurs when the incident particle has penetrated the quantum dot. Therefore, we propose that the dielectric ϵ_{QD} is to be used for *all* incident trajectories with impact parameters less than R, and ϵ_{ce} is to be used otherwise. Thus, Eqs. (C8), (C16), and (C17) are to be used for R_{co} larger than the quantum-dot radius, but [β_{QD} is (C4) evaluated at the quantum-dot radius R]

$$Q_{CPW}(i\rightarrow j)=\left[\frac{m_i}{m_0}\right]\left[\frac{2\sum_{i,j}f_{ji}}{3g_i}\right]\left[\frac{1}{E_{ji}E_{inc}}\right]\left[\frac{e^2}{4\pi\epsilon_{ce}R}\right]^2\left[\phi(\beta_{QD})+\left[\frac{\epsilon_{ce}}{\epsilon_{QD}}\right]^2[\phi(\beta_{co})-\phi(\beta_{QD})]\right](\pi R^2)\,, \tag{C18}$$

$$Q_{CPF}(i\rightarrow j)=\left[\frac{m_i}{m_0}\right]\left[\frac{2\sum_{i,j}f_{ji}}{3g_i}\right]\left[\frac{1}{E_{ji}E_{inc}}\right]\left[\frac{e^2}{4\pi\epsilon_{ce}R}\right]^2\left[\phi(\beta_{qd})+\left[\frac{\epsilon_{ce}}{\epsilon_{QD}}\right]^2[\phi(\beta_{co})-\phi(\beta_{QD})+\tfrac{1}{2}\zeta(\beta_{c9})]\right](\pi R^2)\,, \tag{C19}$$

and

$$Q_{CPT}(i\rightarrow j)=\left[\frac{m_i}{m_0}\right]\left[\frac{2\sum_{i,j}f_{ji}}{3g_i}\right]\left[\frac{1}{E_{ji}E_{inc}}\right]\left[\frac{e^2}{4\pi\epsilon_{ce}R}\right]^2\left[\phi(\beta_{QD})+\left[\frac{\epsilon_{ce}}{\epsilon_{QD}}\right]^2[\phi(\beta_{co})-\phi(\beta_{QD})+\tfrac{1}{3}\zeta(\beta_{co})]\right](\pi R^2) \tag{C20}$$

are to be used when R_{co} is less than R to approximately account for the difference in the quantum dot and barrier dielectrics.

APPENDIX D: THE BINARY ENCOUNTER $P_{BE}(U_i/k_BT, E_2/k_BT)$

The Binary encounter $P_{BE}(U_i/k_BT, E_2/k_BT)$ is defined as

$$P_{BE}\left[u_i=\frac{U_i}{k_BT},\mathcal{E}_2=\frac{E_2}{k_BT}\right]=\int_{u_i}^{\infty}\frac{\mathcal{E}_1 d\mathcal{E}_1\exp(-\mathcal{E}_1)}{\mathcal{E}_1+u_i+\mathcal{E}_2}\left[\left[\frac{1}{u_i}-\frac{1}{\mathcal{E}_1}\right]+\frac{2}{3}\mathcal{E}_2\left[\frac{1}{u_i^2}-\frac{1}{\mathcal{E}_1^2}\right]-\frac{1}{\mathcal{E}_1+u_i}\ln\left|\frac{\mathcal{E}_1}{u_i}\right|\right] \tag{D1}$$

with $\mathcal{E}_1=E_1/k_BT$, $u_i=U_i/k_BT$, and $\mathcal{E}_2=E_2/k_BT$. This integral can be evaluated as

$$\begin{aligned}P_{BE}(u_i,\mathcal{E}_2)=&\frac{\exp(-u_i)}{u_i}-(2u_i+\mathcal{E}_2)\frac{\exp(u_i+\mathcal{E}_2)}{u_i}E_1(2u_i+\mathcal{E}_2)\\&+\frac{2\mathcal{E}_2}{3u_i^2}\left[\exp(-u_i)-\left[\frac{u_i^2}{u_i+\mathcal{E}_2}\right]E_1(u_i)-\frac{\mathcal{E}_2(2u_i+\mathcal{E}_2)}{(u_i+\mathcal{E}_2)}\exp(u_1+\mathcal{E}_2)E_1(2u_i+\mathcal{E}_2)\right.\\&\left.-\int_{u_i}^{\infty}\frac{\mathcal{E}_1 d\mathcal{E}_1\exp(-\mathcal{E}_1)\ln\left|\frac{\mathcal{E}_1}{u_i}\right|}{(\mathcal{E}_1+u_i+\mathcal{E}_2)(\mathcal{E}_1+u_i)}\right].\end{aligned} \tag{D2}$$

A good approximation for the last integral can be made with the help of

$$\begin{aligned}\int_{u_i}^{\infty}\frac{\mathcal{E}_1 d\mathcal{E}_1\exp(-\mathcal{E}_1)\ln\left|\frac{\mathcal{E}_1}{u_i}\right|}{(\mathcal{E}_1+u_i+\mathcal{E}_2)(\mathcal{E}_1+u_i)}=&\left[\frac{\ln\left[\frac{e_F}{u_i}+1\right]}{e_F}\right]\\&\times\exp(-u_i)\left[-1+\exp(2u_i+\mathcal{E}_2)[E_1(2u_i+\mathcal{E}_2)\right.\\&\left.-E_1(e_F+2u_i+\mathcal{E}_2)](2u_i+\mathcal{E}_2)\left[\frac{u_i+\mathcal{E}_2}{\mathcal{E}_2}\right]\right.\\&\left.-\left[\frac{u_i}{\mathcal{E}_2}\right]\exp(2u_i)[E_1(2u_i)-E_1(e_F+2u_i)](2u_i)\right],\end{aligned} \tag{D3}$$

where e_F satisfies $\exp(-e_F)\simeq 0$. For large (normalized) ionization potentials u_i (and small bound energies E_2), the in-

tegral $P_{\mathrm{BE}}(U_i/k_BT, E_2/k_BT)$ in (D2) can be approximated as

$$P_{\mathrm{BE}}(u_i,\mathscr{E}_2)\simeq\frac{\exp(-u_i)}{u_i}\left[\frac{1}{2(2u_i+\mathscr{E}_2)}-\frac{2}{(2u_i+\mathscr{E}_2)^2}\right], \tag{D4}$$

indicating that the tightly bound states have very small collisional ionization rates.

---

*Mailing address: 350 Memorial Drive, Cambridge, MA 02139-4304.

[1]M. G. Bawendi, W. L.Wilson, L. Rothberg, P. J. Carroll, T. M. Jedju, M. L. Steigerwald, and L. E. Brus, Phys. Rev. Lett. **65**, 1623 (1990).

[2]M.G. Bawendi, P. J. Carroll, W. L. Wilson, and L. E. Brus, J. Chem. Phys. **96**, 946 (1992).

[3]M. G. Bawendi, A. R. Kortan, M. L. Steigerwald, and L. E. Brus, J. Chem. Phys. **91**, 7282 (1989).

[4]A. P. Alivisatos, T. D. Harris, P. J. Carroll, M. L. Steigerwald, and L. E. Brus, J. Chem. Phys. **90**, 3463 (1989).

[5]A. P Alivisatos, A. L. Harris, N. J. Levinos, M. L. Steigerwald, and L. E. Brus, J. Chem. Phys. **89**, 4001 (1988).

[6]M. Asada, Y. Miyamoto, and Y. Suematsu, IEEE J. Quantum Electron. **QE-22**, 1915 (1986).

[7]Y. Arakawa and H. Sakaki, Appl. Phys. Lett. **40**, 939 (1982).

[8]K. J. Vahala, IEEE J. Quantum Electron. **QE-24**, 523 (1988).

[9]H. Sakaki, Jpn. J. Appl. Phys. **28**, L314 (1989).

[10]J.-B. Xia, Phys. Rev. B **40**, 8500 (1989).

[11]J. L Pan, Phys. Rev. B **46**, 4009 (1992).

[12]R. W. P. McWhirter, Phys. Rep. **37**, 165 (1978).

[13]A. Burgess and H. P. Summers, Mon. Not. R. Astron. Soc. **174**, 345 (1976).

[14]J. L. Pan (unpublished).

[15]J. L. Pan (unpublished).

[16]Y. Miyamoto, Y. Miyake, M. Asada, and Y. Suematsu, IEEE J. Quantum Electron. **QE-25**, 2001 (1989).

[17]T. Takahashi and Y. Arakawa, IEEE J. Quantum Electron. **27**, 1824 (1991).

[18]J. L. Pan, Phys. Rev. B **46**, 3977 (1992).

[19]*Handbook of Chemistry and Physics,* edited by R. C. Weast (CRC Press, Inc., Boca Raton, FL, 1989).

[20]*Numerical Data and Functional Relationships in Science and Technology,* Landolt-Börnstein, New Series, Vol. 17, Pt. b (Springer-Verlag, New York, 1982).

[21]G. Margaritondo and P. Perfetti, in *Heterojunction Band Discontinuities: Physics and Device Applications,* edited by F. Capasso and G. Margaritondo (Elsevier Science, Amsterdam, 1987).

[22]J. Tersoff, in *Heterojunction Band Discontinuities: Physics and Device Applications* (Ref. 21).

[23]A. D. Katnani, in *Heterojunction Band Discontinuities: Physics and Device Applications* (Ref. 21).

[24]H. Van Regemorter, Astrophys. J. **136**, 906 (1962).

[25]M. J. Seaton, Proc. Phys. Soc. **79**, 1105 (1962).

[26]K. Alder, A. Bohr, T. Huus, B. Mottelson, and A. Winther, Rev. Mod. Phys. **28**, 432 (1956).

[27]H. Massey and B. Moiseiwitsch, Phys. Rev. **78**, 180 (1950).

[28]C. Erginsoy, Phys. Rev. **79**, 1013 (1950).

[29]S. S. Hsuang, Phys. Rev. **76**, 477 (1949).

[30]S. G. Elkomoss and G. Munschy, J. Phys. Chem. Solids **40**, 431 (1979). The cross sections in Fig. 7 of their work depict only half of the total 1*s*-2*p* cross section. We thus doubled their numerical values to obtain the curve labeled *G* in our Fig. 3.

[31]H. Tai, R. H. Bassel, E. Gerjuoy, and V. Franco, Phys. Rev. A **1**, 1819 (1970).

[32]A. Honold, L. Schultheis, J. Kuhl, and C. W. Tu, Phys. Rev. B **40**, 6442 (1989).

[33]L. Schultheis, J. Kuhl, A. Honold, and C. W. Tu, Phys. Rev. Lett. **57**, 1635 (1986).

[34]J. D. Jackson, *Classical Electrodynamics* (Wiley, New York, 1975).

[35]S. Schmitt-Rink, D. A. B. Miller, and D. S. Chemla, Phys. Rev. B **35**, 8113 (1987).

[36]A. Burgess and J. A. Tully, J. Phys. B **11**, 4271 (1978).

[37]B. K. Ridley, *Quantum Processes in Semiconductors* (Oxford University Press, New York, 1988).

[38]G. P. Agrawal and N. K. Dutta, *Long Wavelength Semiconductor Lasers* (Van Nostrand Reinhold, New York, 1986).

[39]P. L. Hagelstein (unpublished).

[40]Ch. Nöldeke, W. Metzger, R. P. Huebener, and H. Schneider, Phys. Status Solidi B **129**, 687 (1985).

[41]T. Yao, K. Inagaki, and S. Maekawa, Solid State Commun. **13**, 533 (1973).

[42]J. Yamashita, J. Phys. Soc. Jpn. **16**, 720 (1961).

[43]L. Vriens, in *Case Studies in Atomic Collision Physics I,* edited by E. W. McDaniel and M. R. C. McDowell (Wiley, New York, 1969), p. 335.

[44]L. Vriens, Proc. Phys. Soc. **89**, 13 (1966).

[45]M. R. C. McDowell, Proc. Phys. Soc. **89**, 23 (1966).

[46]J. S. Hansen, Phys. Rev. A **8**, 822 (1973).

[47]P. C. Sercel and K. J. Vahala, Phys. Rev. B **42**, 3690 (1990).

[48]E. O. Kane, J. Phys. Chem. Solids **1**, 249 (1957).

[49]A. R. Beattie and P. T. Landsberg, Proc. R. Soc. London Ser. A **219**, 16 (1959).

[50]A. Haug, D. Kerkhoff, and W. Lochmann, Phys. Status Solidi B **89**, 357 (1978).

[51]Y. L. Luke, *Integrals of Bessel Functions* (McGraw-Hill, New York, 1962).

[52]M. Rotenberg, R. Bivins, N. Metropolis, J. K. Wooten, Jr., *The 3-j and 6-j Symbols* (Technology Press, Cambridge, MA, 1959).

[53]*Handbook of Mathematical Functions with Formulas, Graphs, and Mathematical Tables,* edited by M. Abramowitz and I. A. Stegun (National Bureau of Standards, Washington, D.C., 1964).

[54]N. F. Mott and H. S. W. Massey, *The Theory of Atomic Collisions* (Clarendon, Oxford, 1965).